1979-09

# Induced evaporation of metal from an aluminum surface by a normal pulse neodymium laser

Johnson, Christopher Brinton

Monterey, California. Naval Postgraduate School

# INDUCED EVAPORATION OF METAL FROM AN ALUMINUM SURFACE BY A NORMAL PULSE NEODYMIUM LEVEL

Christopher Brinton Johnson

# NAVAL POSTGRADUATE SCHOOL
## Monterey, California


# THESIS

INDUCED EVAPORATION OF METAL
FROM AN ALUMINUM SURFACE
BY A NORMAL PULSE NEODYMIUM LASER

by

Christopher Brinton Johnson

September 1979

Thesis Advisor: F. Schwirzke

Approved for public release; distribution unlimited.

## REPORT DOCUMENTATION PAGE

READ INSTRUCTIONS BEFORE COMPLETING FORM

1. REPORT NUMBER
2. GOVT ACCESSION NO.
3. RECIPIENT'S CATALOG NUMBER

4. TITLE (and Subtitle)
Induced Evaporation of Metal From an Aluminum Surface by a Normal Pulse Neodymium Laser

5. TYPE OF REPORT & PERIOD COVERED
Master's Thesis; September 1979

6. PERFORMING ORG. REPORT NUMBER

7. AUTHOR(s)
Christopher Brinton Johnson

8. CONTRACT OR GRANT NUMBER(s)

9. PERFORMING ORGANIZATION NAME AND ADDRESS
Naval Postgraduate School
Monterey, California 93940

10. PROGRAM ELEMENT, PROJECT, TASK AREA & WORK UNIT NUMBERS

11. CONTROLLING OFFICE NAME AND ADDRESS
Naval Postgraduate School
Monterey, California 93940

12. REPORT DATE
September 1979

13. NUMBER OF PAGES
76

14. MONITORING AGENCY NAME & ADDRESS(if different from Controlling Office)

15. SECURITY CLASS. (of this report)

15a. DECLASSIFICATION/DOWNGRADING SCHEDULE

16. DISTRIBUTION STATEMENT (of this Report)

Approved for public release; distribution unlimited.

17. DISTRIBUTION STATEMENT (of the abstract entered in Block 20, if different from Report)

18. SUPPLEMENTARY NOTES

19. KEY WORDS (Continue on reverse side if necessary and identify by block number)

Laser Induced Evaporation
Neodymium Laser

20. ABSTRACT (Continue on reverse side if necessary and identify by block number)

Laser induced evaporation of material from the surface of an aluminum target in a vacuum was studied. Based on a literature examination, material removal using a normal pulse laser was judged to be more efficient than for a Q-switched laser. The experiment was conducted using a neodymium glass laser modified for normal pulse operation. The energy density was varied from $8.5 \times 10^{2}$ J/cm$^2$ where no breakdown occurred to $5 \times 10^{3}$ J/cm$^2$ where the threshold for

#20 - ABSTRACT - CONTINUED

breakdown was exceeded. The normal pulse duration was 600 μs. Analysis of the ejected material was achieved by using a Hughes Ionization Gauge placed in the path of the ejected material. Oscilloscope traces of the ionization gauge output show that the gauge "sees" what is flying past it. There is good correlation between laser radiation, plasma radiation and ionization gauge fluctuations. The ionization gauge gave distinguishable signals for ions, electrons, and neutral particles ejected from the target surface. Signal sequence was dependent on the particle velocity. By measuring the elapsed time after ejection from the surface and the target to collector distance, the first arriving neutral particle velocity was determined to be $5.2 \times 10^4$ cm/s.

Approved for public release; distribution unlimited.

# Induced Evaporation of Metal from an Aluminum Surface by a Normal Pulse Neodymium Laser

by

Christopher Brinton Johnson
Major, United States Army
B.A., Washington State University, 1968
M.S., University of Southern California, 1975

Submitted in partial fulfillment of the
requirements for the degree of

MASTER OF SCIENCE IN PHYSICS

from the

NAVAL POSTGRADUATE SCHOOL

September 1979

## ABSTRACT

Laser induced evaporation of material from the surface of an aluminum target in a vacuum was studied. Based on a literature examination, material removal using a normal pulse laser was judged to be more efficient than for a Q-switched laser. The experiment was conducted using a neodymium glass laser modified for normal pulse operation. The energy density was varied from $8.5 \times 10^2$ J/cm$^2$ where no breakdown occurred to $5 \times 10^3$ J/cm$^2$ where the threshold for breakdown was exceeded. The normal pulse duration was 600 μs. Analysis of the ejected material was achieved by using a Hughes Ionization Gauge placed in the path of the ejected material. Oscilloscope traces of the ionization gauge output show that the gauge "sees" what is flying past it. There is good correlation between laser radiation, plasma radiation and ionization gauge fluctuations. The ionization gauge gave distinguishable signals for ions, electrons, and neutral particles ejected from the target surface. Signal sequence was dependent on the particle velocity. By measuring the elapsed time after ejection from the surface and the target to collector distance, the first arriving neutral particle velocity was determined to be $5.2 \times 10^4$ cm/s.

TABLE OF CONTENTS

ACKNOWLEDGMENT

I wish to thank Robert Sanders, Technician, for his valuable assistance in calibrating and repairing the equipment necessary for this experiment. I would like to extend my sincere gratitude to Professor Schwirzke for his help and guidance throughout the experiment. His comments, suggestions, and academic assistance, during the writing of the thesis, were of great benefit. This work was supported by the Defense Nuclear Agency, MIPR Number 79-512.

# I. INTRODUCTION

A wire explosion is a complex phenomenon resulting from very rapid electrical heating of a piece of metal which has a small cross sectional area. The wire is heated and undergoes phase change. There is a bright flash of light and a loud report (in air). Thus, the term "exploding wire" has been coined to describe this phenomenon. More appropriately, the term "exploding conductor" will be used to denote the explosion of a single wire, a multiple wire array, a metal foil, or a gas puff by a high current pulse. This technique is a relatively simple way of generating a plasma, which can be used to study the dense plasma itself or for further experimental work such as spectroscopy.

The idea of exploding conductors is not a new one [3]. As early as 1773, Edward Nairne conducted experiments exploding a .15 mils diameter iron wire in proving that current in all parts of a series circuit is the same [45]. Eighty years later, Michael Faraday reported on wire explosions used to produce a metal film or mirror. The use of exploding wires was of little importance until the work of John A. Anderson in the 1920's. At Mt. Wilson Observatory, he showed that the temperatures involved approached those of the sun, in excess of 3000°C [48]. In the years that followed, research on exploding conductors was principally conducted by Nabaoka, Kleen, Wrana, Eiselt, Conn, Kvartskhava

and Lebedev [3]. Since 1950, exploding conductors have become a matter of great scientific interest. Perhaps the largest number of researchers to use exploding conductors have capitalized on the extremely short, intense light output. These intense pulses of light have been used in spectroscopy and high speed photography, as well as in radiation chemistry and laser technology as an excitation source for coherent radiation [50].

Other uses of exploding conductors are the production and study of aerosols, production of thin metal films [27], silvering of mirrors, and chemical synthesis [1]. In the past 10-12 years, the use of exploding conductors as bridge-type electrical detonators has found widespread application both as a method for multi-point detonation of explosives [46] and as a method to generate shock waves in different materials [9]. Another area of intense research, and one in which this paper is related to, is the use of exploding conductors in simulating nuclear weapons effects. In recent years, progress has been made in the development of exploding conductors as x-ray (photon) sources for use in simulating nuclear weapons effects on various satellite "black boxes".

The emission of electromagnetic radiation is a result of suddenly electrically heating thin wires. Four conferences held between 1958 and 1967 dealt exclusively with this subject [17,18,19,20]. Toward this end, several variations of the exploding conductor approach to high energy photon generation have been explored in the past few years.

Single and multiple wire arrays [8,47], cylindrical foils [60], and gas puffs have all been tried to date with limited success. The energy of the emitted x-rays has been too low to be used in nuclear explosion simulations. The problem centers around insufficient energy being coupled to the plasma to allow for radiation in the x-ray region.

Whatever the application or shapes of the conductor, the electrical circuit and the components are similar and perform similar functions, the only difference being in size and characteristics. Each circuit contains an energy storage device, a switch or triggering device, and an explosive conductor. The energy storage device may be a bank of large capacitors or special multiterawatt generators, such as Pithon at Physics International, Gamble II at the Naval Research Laboratory, or Blackjack IV at Maxwell Laboratories, Inc., [63]. These devices are capable of producing 100 KJ pulses of 50-75 nanosecond duration. This high rate of energy release requires special switching devices and transmission lines. Basically, a Marx-capacitor bank (200-300 KJ) is used to charge a single, large, water capacitor. This capacitor discharges into a water dielectric coaxial transmission line that tapers to a 1-2Ω output resistance at the point where the pulse is extracted into a vacuum diode. Thin wires, ribbons or foils are stretched between the electrode gap in the diode [41]. In the case of a wire (13,29,52,53,68] or a foil [66], the initial part

of the electrical discharge causes the conductor to rapidly vaporize uniformly along its entire length. The plasma so formed is then compressed in a Z-pinch. As a result, the plasma consists of "pinched" and "flared" structures characteristic of the m = 0 sausage instability to which Z-pinches are susceptible. It is from these pinched and flared areas that radiation is emitted [22]. Gas puff experiments conducted at Physics International are similar to the exploding conductor ones just described except that a gas puff is substituted for the wires. In addition, the gas puff is ionized with microwaves prior to the arrival of the electrical pulse to insure conductivity of the gas.

Most of the methods giving rise to electromagnetic radiation emitted by plasmas are atomic in nature, that is, they are due to transitions involving bound or free states of atoms or ions. There are three basic methods of energy radiation: bremsstrahlung, recombination radiation, and discrete radiation. Bremsstrahlung or free-free radiation occurs when a free electron collides with an ion or neutral particle and makes a transition to another free state of lower energy with the emission of a photon. The energy of the photon may amount to any fraction of the initial kinetic energy of the electron, $KT_e$; therefore, the bremsstrahlung has a continuum of frequencies determined by $KT_e$. At $T_e = 10^4$ °K, the bremsstrahlung lies in the visible and infrared regions, while at $T_e = 10^8$ °K most of the radiation lies in the x-ray region. Recombination occurs when a

free electron is captured by an n-times ionized atom and makes a transition to a bound state of the (n-1) times ionized atom. The surplus energy is emitted as recombination or free-bound radiation. The energy is equal to the sum of the kinetic energy of the free electron, $KT_e$, and its binding energy. Since free electrons have a continuous energy spectrum, the photons emitted form a continuous energy spectrum. Discrete radiation or bound-bound radiation occurs when a bound electron of an atom or ion is excited to a higher energy state by particle collisions. When the electron returns to a lower state, it yields energy at various discrete frequencies. Whenever a plasma contains ions that have not been completely stripped of orbital electrons, this radiation will appear. Generally, it takes greater plasma energy to completely strip atoms or molecules with higher atomic numbers. As the electron temperature is increased more tightly bound electrons are removed. This will be associated with an increase in the excitation energy of the ions. As a result, the line spectrum will shift from the visible to the x-ray region. Although the radiation emitted from exploding conductors is a combination of the above processes, it is dominated at high temperatures by bremsstrahlung and discrete radiation in the x-ray region [30,34].

The spectral yields and hardness of the emitted radiation from exploding conductors depends on the ionic state and the electron temperature which in turn are influenced by a

combination of competing physical processes. Principal among these are the available generator power, the magneto-hydrodynamic fluid motion of the wire plasma, the coupling of the wire plasma to the driving electrical circuit and the atomic physics and energetics of the plasma. The z-number, geometry and mass of the wire material also play an important role in the above process. A good deal of the understanding of how these competing processes affect the dynamic and radiative behavior of the wire plasma is obtained from experimental data. In addition, computer codes such as WHYRAC [51] have been developed to calculate the detailed time history of the wire implosion. The codes provide insight into the coupling of plasma to the generators and into the energetics of the implosion. Although many of the processes are fairly well understood, their relationship and affect on one another is not.

It is theorized that one way to obtain x rays with the desired characteristics may be to use materials with different, higher z values or even combinations of materials. Many materials can not be fabricated into thin wires or do not have a high enough vapor pressure to allow the formation of a vapor. In response, investigators have therefore proposed that the vapor puffs be generated by using a laser. One of the vacuum diodes would be fabricated out of the target material. The target electrode, irradiated by the laser, would experience a steady temperature rise. If the

laser beam is intense enough, the surface of the target would melt and begin to vaporize. The vapor expands, exposing fresh target layers to heating and vaporization. Depending on the laser intensity, the vapor may remain un-ionized or a plasma may be generated. The high voltage, high current pulse from the Marx-generator would then be timed to pass through the cloud of plasma, neutral particles and molten metal. This procedure advances the possibility of using virtually any material or combination of materials, in addition to being able to vary the mass and temperature of the vapor cloud by varing the power and intensity of the laser pulse.

As indicated earlier, one important parameter on which the dynamics of the z-pinch and x-ray emission depends is the mass of the pinched column. This thesis investigates the mass of material which is blown off a surface as a function of the laser parameters and a method by which it can be measured. Aluminum was selected as the initial target material because of the extensive work done with aluminum exploding wires, thus facilitating a comparison of the two methods in the future.

## II. THEORY

The effect caused by the absorption of high power laser radiation on the surface of an opaque solid slab includes surface heating, melting and vaporization. If the laser intensity is low enough the vapor is un-ionized and remains transparent to the incoming laser radiation. At higher intensities, the vapor becomes ionized generating a plasma. Throughout this thesis, I will use the term "vapor" to denote an ejected cloud of material which contains both neutral particles and plasma. In conjunction with the radiation impinging on the opaque surface, a cycle of events occurs. This is depicted in Figure 1. Prior to considering these events individually, a few comments on lasers in general are appropriate.

First, lasers can be divided into two categories, pulsed and continuous. Only pulsed lasers were considered in this study. Pulsed lasers, in turn, may be subdivided into normal pulse and Q-switched depending on pulse operation. A normal pulse laser is one which is pumped by a flashlamp and the radiation allowed to emerge when the threshold conditions for lasing are reached. Normal pulse lasers emit in pulses lasting tens of milliseconds with peak powers of $10^4$ to $10^5$ watts. The term Q-switched laser denotes lasers employing an element of variable loss within the cavity and emitting peak powers greater than $10^8$ watts and lasting

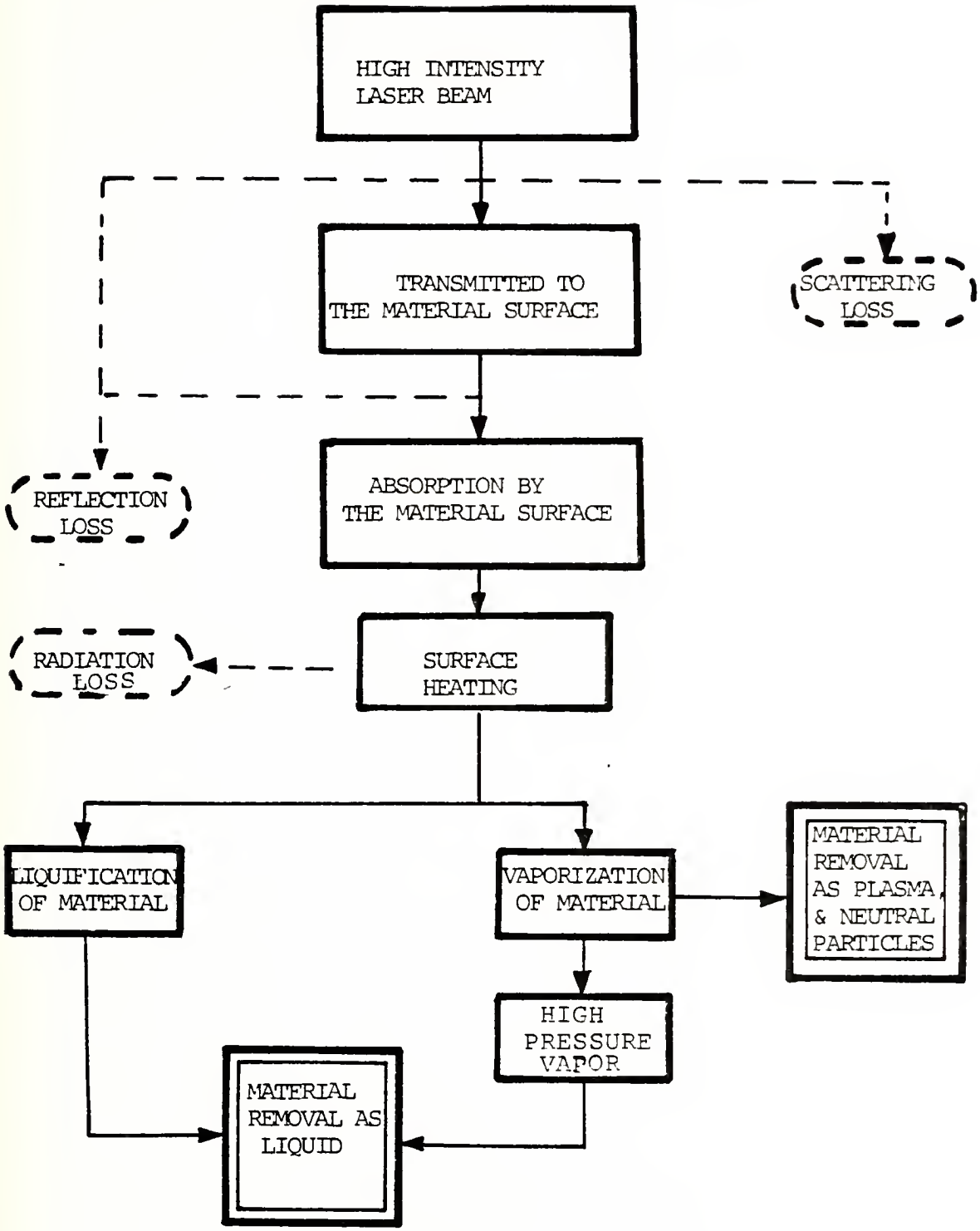


Figure 1. Events diagram for laser-target interaction. Dotted boxes are considered negligible or do not contribute to the study at hand and will not be considered. For simplicity, feedback mechanisms between processes are not included.

several tens of nanoseconds. With Q-switched lasers, flux densities in excess of $10^9$ watts/cm$^2$ are easily attained. In this regime, the vaporization temperature of any metal will be reached in less than one nanosecond. At this point, the input energy begins to supply the latent heat of vaporization to a thin layer of material at the surface and breakdown (avalanche ionization) will occur. During breakdown, the few naturally occurring thermal electrons from the target surface are heated by the laser beam. They will gain energy until they are capable of ionizing neutral particles by collision. Each collision will produce ions and more electrons which will also be heated by the laser beam to the point where they too can ionize neutral particles. The process thus continues exponentially producing electrons and ions and absorbing more and more of the laser radiation. The "breakdown threshold" is the laser intensity required to generate a high density plasma at the target surface. Experiments have shown that breakdown over a laser-irradiated surface exhibits a sharp threshold in laser intensity. Several models have been developed that predict this breakdown threshold [40,54]. Below threshold, insufficient energy is available to propogate the avalanche ionization and the vapor remains relatively transparent. When the breakdown threshold is reached, a high absorption plasma cloud is formed on the target surface. For example, consider Q-switched neodymium-glass laser radiation (1.06 μm) incident upon an aluminum

target. A typical pulse could have a flux of $10^9$ to $10^{10}$ watts/$cm^2$ and a duration of 10-100 nanoseconds. Figure 2, taken from Ref. 4 models the relationship between the threshold intensity required for breakdown and the laser pulse duration. The prediction is that breakdown will occur in this case. Because of breakdown, the energy in the beam is devoted to heating a small amount of vaporized material to a high temperature, while the heat transfer from the hot vapor to the bulk of the target material is limited due to the short pulse duration. A normal pulse laser has a series of spikes, many of which are capable of producing breakdown. The difference is that the individual spikes do not possess enough intensity to perpetuate the ionization process. The vapor is heated, breakdown occurs and absoprtion of energy increases, but the laser spike intensity falls off rapidly and breakdown ceases. This process is repeated many times resulting in more energy being coupled to the target and thus more material being ejected. Consequently, a given amount of energy delivered at very high power is less effective in causing vaporization than the same amount of energy delivered in a longer, lower power pulse. It is for this reason that only normal pulse lasers were considered in this thesis.

## A. REFLECTIVITY

When one considers the coupling of laser radiation to the surface of a target, one first needs to know how much energy is absorbed into the material. The Drude-Lorentz free

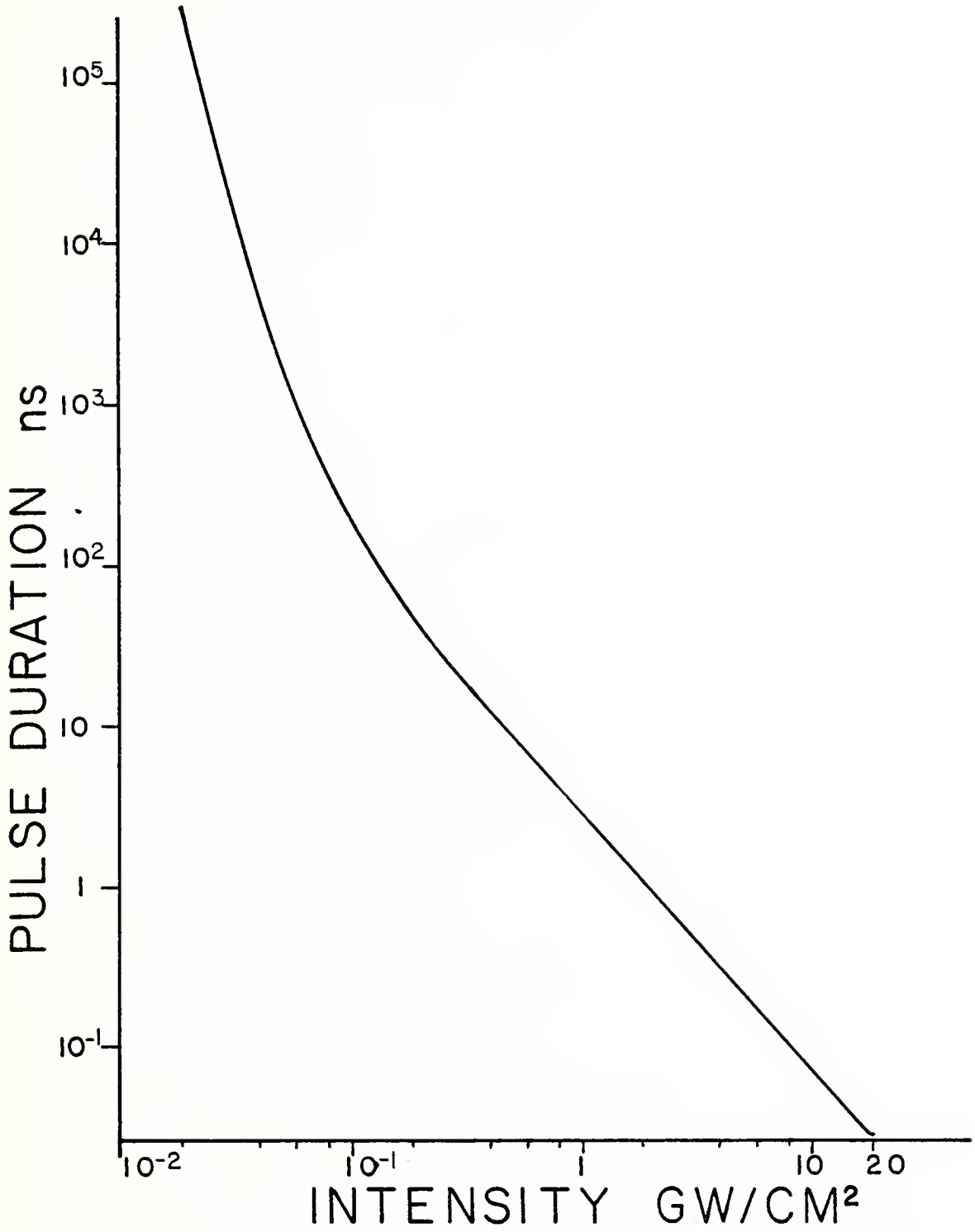


Figure 2. Pulse duration time vs breakdown threshold intensity for an aluminum target irradiated by a 1.06 μm laser pulse. Alternatively, this graph gives the breakdown time vs peak value of incident laser beam intensity. Taken from Ref. 4.

electron theory provides an acceptable model for metals interacting with infrared wavelength photons [66]. According to the model, electromagnetic radiation interacts only with free electrons in a metal. The absorbed photon energy raises electrons to higher energy states in the conduction band. The excited electrons, in turn, collide with lattice phonons and other electrons as they give up their energy. The electron-phonon collision frequency is proportional to the phonon population in the metal. The phonon population, on the other hand, determines the temperature of the metal. Thus, the rise in temperature strongly affects the electron-phonon collision frequency which in turn affects the reflectivity of the metal. Based on the Drude-Lorentz theory several authors have developed theoretical expressions that predict the absorbtivity of metals [49,66].

The reflectivity of a "real metal" surface is largely an empirical matter. Bonch-Bruevich et al. [10] investigated the reflectivity at 1.06 μm of aluminum, copper, dural, steel, and silver as the metals were irradiated with a laser beam. The investigators surrounded the sample with a sphere to monitor the reflected radiation, Figure 3. Pronounced changes both during each individual spike and over the pulse as a whole were reported. Figure 4 shows the generalized reflectivity behavior of a metal during an individual spike. The region of rapid change of reflectivity a-b is due to initial heating of the metal. The segment b-c has a constant reflectivity which the authors attributed to the constant temperature during the time when the melting wave is propagating into the metal. Zavecz [71],

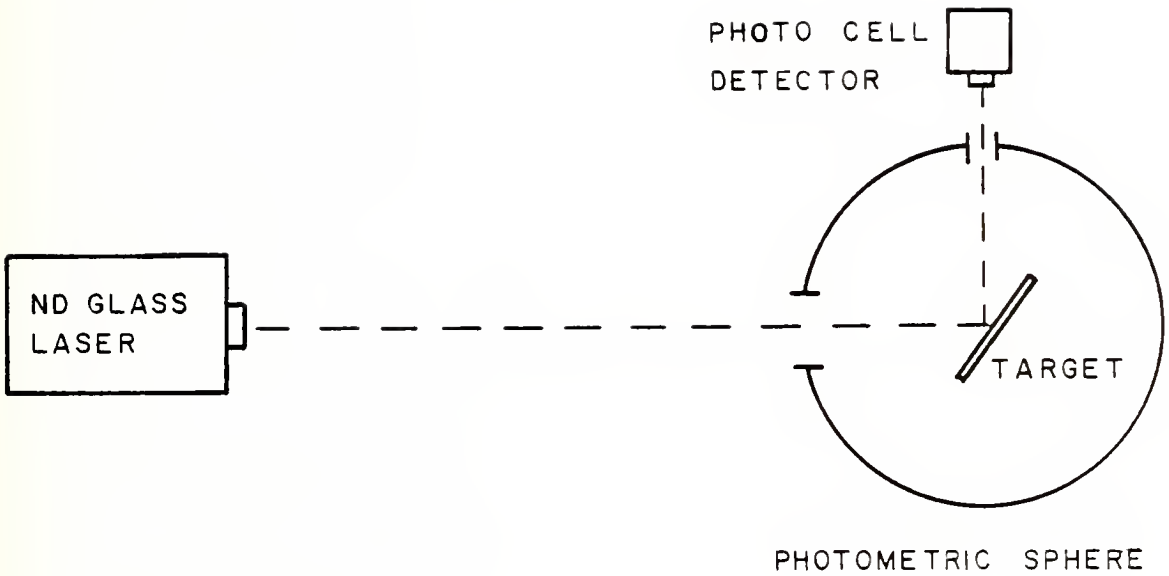


Figure 3. Schematic of the apparatus used by Bonch-Bruevich, et al. [10] for measuring the change in reflecting power of a metal under the action of laser radiation.

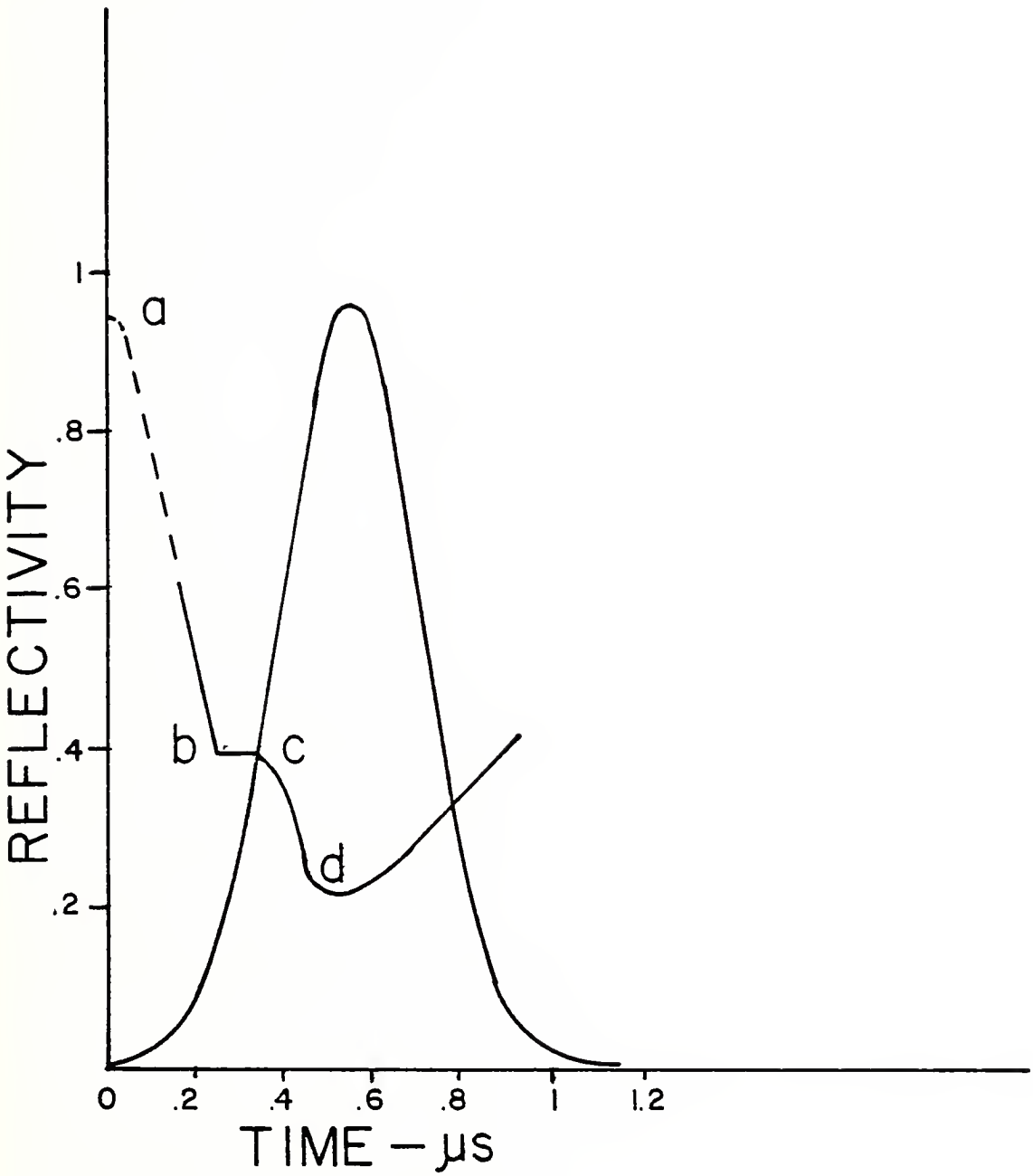


Figure 4. Change of reflecting power of silver at 1.06 μm during a single spike. The form of the laser spike with energy of 7.5 KJ/cm$^2$ is also depicted [10].

disagreeing, feels that this low reflectivity plateau is a function of the instantaneous pulse intensity and the specimen's equilibrium temperature. Finally, the surface temperature begins to rise again, thus causing a further drop in reflectivity, segment c-d. The increase in reflectivity to the right of point d is due to the decay of the spike flux density and the subsequent drop in temperature. Similar results were published by Chun and Rose [21] as reflected in Figure 5. In addition, Chun and Rose examined the dependence of absorptance on the depth (internal volume) of the laser crater. These results, depicted in Figure 6, indicate that absorptance changes as the depth of the crater changes. This means that even if the initial reflectivity is high, much of the energy in a focused normal pulse laser will be absorbed by a metal surface. Although only experimental results for incident radiation at 1.06 μm has been described, experimental work at other wavelengths has been done [57]. In all cases the experimental observations show that under high-intensity radiation, metal absorptivity increases non linearly.

## B. HEATING OF THE MATERIAL

Possibly one of the most important effects of intense laser irradiation is the conversion of optical energy in the beam into thermal energy in the material. The radiation mean free path for visible and infrared wavelengths in a solid material such as a metal, is typically of the order of $10^{-4}$ cm or less, so that the deposition of laser energy can be considered

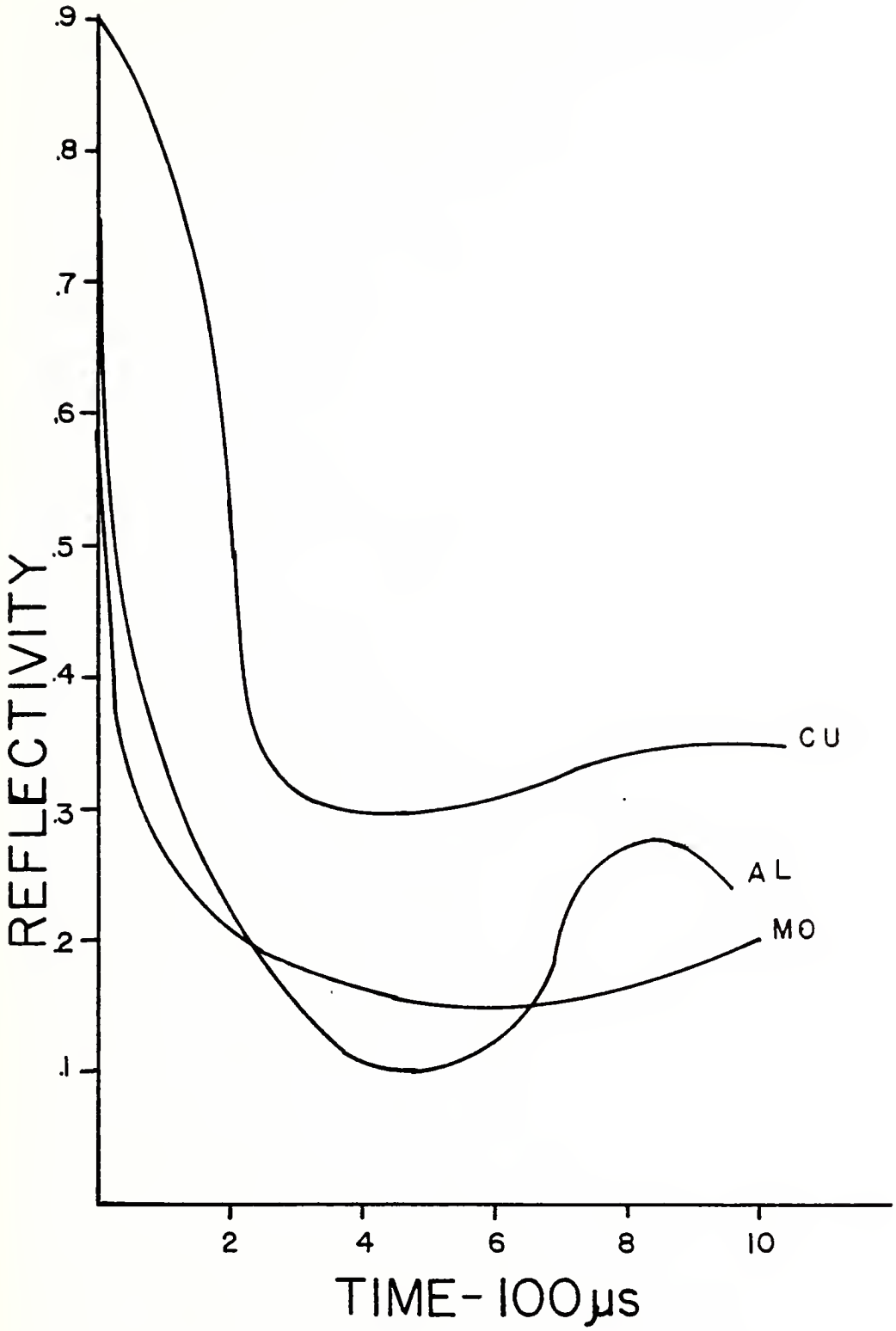


Figure 5. Time dependent reflectance measurement at 1.06 μm from Ref. 21. A single laser pulse with a power density of $10^7$ W/cm$^2$ was used.

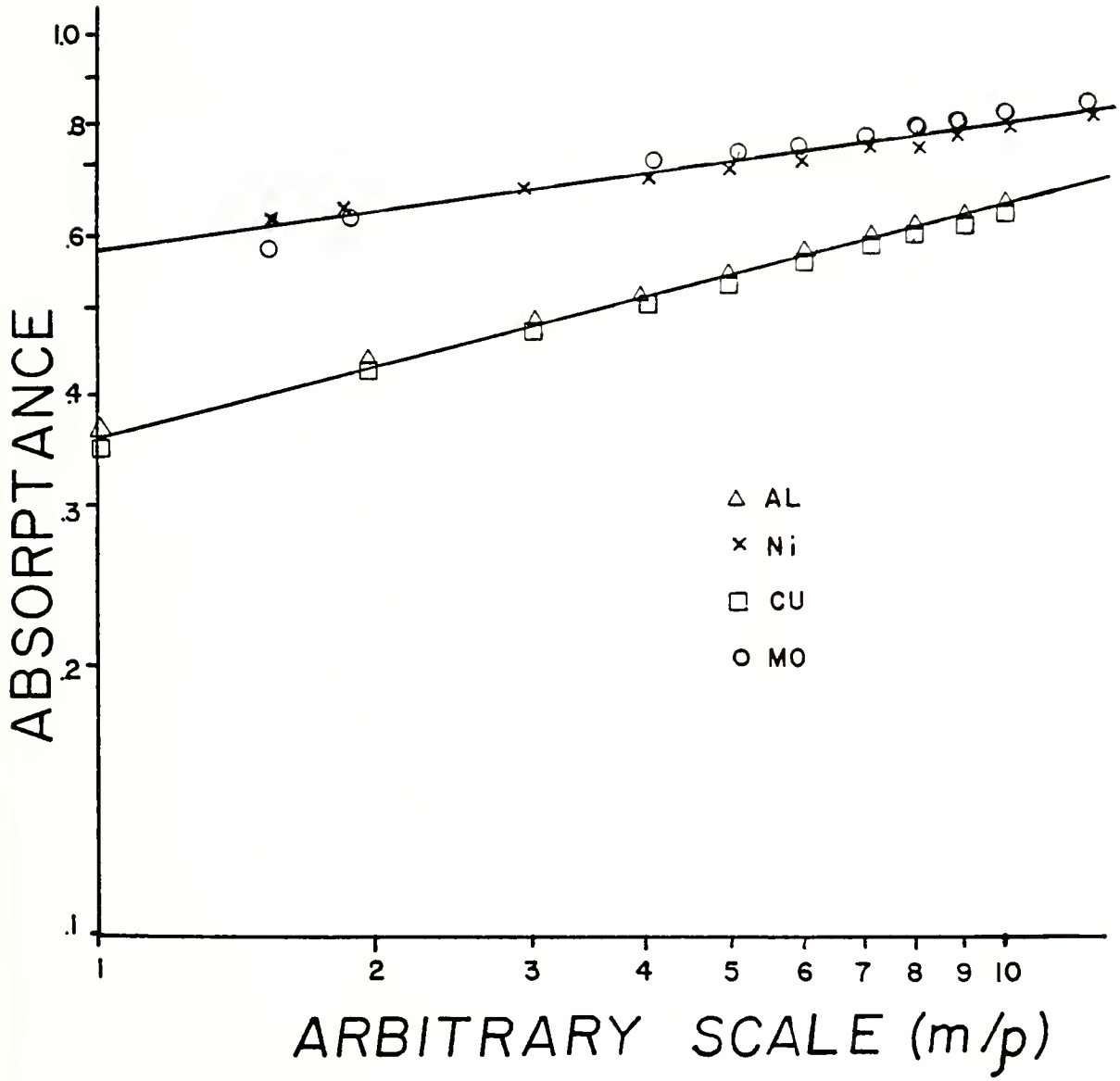


Figure 6. Dependence of absorbtance at 1.06 μm on crater volume from Ref. 21. m/ρ is the ratio of mass removed to material density.

to be a surface phenomenon insofar as the transport of energy in a solid is concerned. The Drude-Lorentz free electron theory as previously discussed is the basis of thermal response of the material. The time required (relaxation time) for electrons, excited by irradiation, to transfer their energy to the lattice by means of electron-phonon collisions amounts to approximately $10^{-11}$ sec [36,72,74]. When compared to a laser pulse, the relaxation time is short, allowing one to assume that the heat transfer to the solid is instantaneous because local equilibrium is rapidly established. Therefore, one is justified in assuming that temperature is a valid concept and so the normal equations of heat flow may be applied. The following development has been principally adapted from Harrach [30,32], but other authors have similar developments [7,49].

Suppose that at time t = 0 laser radiation is directed upon an opaque, solid slab of metal. A portion of the radiation, is absorbed; the rest being reflected as described in the previous section. A temperature distribution T(r,t) develops throughout the material. When a temperature gradient exists in a body, there is an energy transfer from the high-temperature region to the low-temperature region. The heat conduction equation (without phase changes) is [15]

$$\nabla \cdot J(r,t) + PC \frac{\partial T(r,t)}{\partial t} = A(r,t) \qquad (1)$$

where T(r,t) is the temperature, J(r,t) is the thermal energy crossing unit area per unit time, $\rho c$ is the heat capacity per unit volume, and A(r,t) is the net heat energy per unit volume time generated. Fourier's law relates the temperature to the heat flux

$$J(r,t) = -K\nabla T(r,t) \tag{2}$$

To simplify the calculations, it is assumed, as in Refs. 4 and 59, that the problem is planar, heat is introduced only from the surface and flows into the material in the x-direction. The thermophysical constants are independent of temperature, radiation and convection from the surface is negligible, and the liquid phase of the material can be ignored. The heat flow can now be modeled using the Fourier heat-conduction equation [54]

$$\frac{\partial^2 T(x,t)}{\partial x^2} + \frac{1}{K} A(x,t) = \frac{1}{k} \frac{JT(x,t)}{\delta t} \tag{3}$$

where k is the thermal diffusion constant equal to $\rho KC$ and K is the thermal conductivity constant. The rate of heat production can be written as

$$A = \frac{\alpha I}{\rho C \delta} \tag{4}$$

where $\alpha$ is the surface absorptivity, I is the flux density of the incident radiation, $\delta$ is the penetration skin depth of

radiation into the target material, $\rho$ is the density of the target material, and C is the specific heat. Now by substitution of (4) into (3), the model equation becomes

$$- k \frac{\partial^2 T(x,t)}{\partial x^2} + \frac{\partial T(x,t)}{\partial t} = \frac{\alpha I(x,t)}{PC\delta} \qquad (5)$$

In order to solve this differential equation, the various parameters must be known or at least estimated. With the exception of $\delta$, each parameter has an accepted value which can be used. The value for $\delta$ is not so easy to determine. It is expected to be small, $10^{-6}$ cm [74]. It can be assumed that the laser radiation is absorbed in an infinitesimally thin surface layer ($\delta \rightarrow 0$). The source term may now be deleted from (5). The term is not lost however, since it will be incorporated into the surface boundary conditions. Equation (5) now becomes

$$- K \frac{\partial^2 T(x,t)}{\partial x^2} + \frac{\partial T(x,t)}{\alpha t} = 0 \qquad (6)$$

The specific boundary conditions depend on whether the surface of the target is being vaporized or not. For the case at hand, no vaporization, the surface boundary condition is

$$- K \frac{JT(x,t)}{\partial x} = \frac{\alpha I(t)}{\rho C} \quad \text{for } x = 0$$

or

$$K \frac{\partial T(x,t)}{\partial x} = \alpha I(t) \tag{7}$$

A second boundary condition arises when the target is considered to be a semi-infinite solid.

$$\lim_{x \to \infty} \frac{\partial T(x,t)}{\partial x} = 0 \tag{8}$$

And finally, the third condition is

$$T(x,0) = 0 \tag{9}$$

In general, equation (6) does not yield an exact solution. One method of solution, utilized by Harrach, is the "heat balance integral method" [30]. This method, which is based on the assumption that "the partial differential equation is required to be satisfied only in an average sense throughout the solid rather than at each point x," is outlined below. The integral method reduces the nonlinear boundary value problem to an ordinary initial value problem where solutions can be expressed in closed analytical form.

Integrating eqution (6) over the spatial interval of the target, $x_s \leq x \leq \ell$ gives

$$\int_{x_s}^{\ell} k \frac{\partial^2 T}{\partial x^2} dx = \int_{x_s}^{\ell} \frac{\partial T}{\partial t} dx \tag{10}$$

In general taking the derivative of an integral yields

$$\frac{d}{dt} \int_{x_s}^{\ell} T \, dx = \int_{x_s}^{\ell} \frac{\partial T}{\partial t} dx + T(x = \ell, t) \frac{d\ell}{dx} - T(x = x_s, t) \frac{dx_s}{dt} \tag{11}$$

Using equation (10) and the results of equation (11), noting $d\ell/dt = 0$ and assuming k is constant

$$k\left(\frac{\partial T}{\partial x}\Big|_{x=\ell} - \frac{T}{x}\Big|_{x=x_s}\right) = \frac{d}{dt} \int_{x_s}^{\ell} T \, dx + T(x_s, t) \frac{dx_s}{dt} \tag{12}$$

If the target surface is stationary then $dx_s/dt = 0$. Goodman [26] points out that the key step in the careful choice of the solution form, T(x,t). The idea is to choose T(x,t) such that it can be integrated explicitly. This gives an ordinary first order differential equation when substituted into equation (12). Now to apply this technique to the problem defined by equation (6) and the boundary conditions (7), (8), and (9)

$$\frac{d}{dt} \int_{0}^{\ell} T(x,t) dx = \frac{k\alpha I(t)}{K} \tag{13}$$

Consider the solution form

$$T(x,t) = T(0,t)[1 - x/\xi(t)]^2 \exp[-x/\xi(t)], \quad \text{for } 0 \leq x \leq \xi(t) \tag{14}$$

and

$$T(x,t) = 0 \quad \text{for } x \geq \xi(t)$$

where $T(0,t)$ is the front surface temperature and $\xi(t)$ is a time dependent thermal penetration depth. Integrating equation (14) over x from 0 to $\ell$ and incorporating equation (13) yields the ordinary differential equation

$$\frac{d}{dt}[T(0,t)\xi(t)] = [k\alpha I(t)]/[1-2e^{-1}]K \tag{15}$$

Substituting equation (14) into equation (7) gives

$$\xi(t) = 3KT(0,t)/\alpha I(t) \tag{16}$$

Solving equations (15) and (16) simultaneously yields

$$T(0,t) = \left(\frac{k}{3(1-e2^{-1})K^2}\right)^{1/2} \left(\alpha I(t) \int_0^t I(t')dt'\right)^{1/2} \tag{17}$$

and

$$\xi(t) = \left(\frac{3k}{1-2e^{-1}}\right)^{1/2} \left(\int_0^t \frac{\alpha I(t')dt'}{\alpha I(t)}\right)^{1/2} \tag{18}$$

Several special cases can now be considered by stipulating the laser profile I(t) and the dependence of the absorptivity on temperature, $\alpha = \alpha(t)$.

CASE 1:

Let the absorptivity coefficient be constant, $\alpha_o$, and the laser pulse be a step function. The solution to equation (17) is now found to be

$$T(0,t) = \frac{\alpha_o I_o}{k}\left(\frac{kt}{3(1-2e^{-1})}\right)^{1/2} \tag{19}$$

and from equation (18)

$$\xi(t) = \left(3KT/(1-2e^{-1})\right)^{1/2} \tag{20}$$

For comparison, the exact solution as outlined by Carslaw and Jaeger [61] is

$$T(x,t) = \frac{2\alpha I_o}{K}\left(\frac{kt}{\pi}\right)^{1/2}\left\{\frac{x}{4(\pi kt)^{1/2}} \exp(-x^2/4kt) - \frac{1}{2}\operatorname{erfc}[x/(4\pi t)^{1/2}]\right\} \tag{21}$$

In the above equation erfc denots the complementary function

$$\text{erfc}(\lambda) = 1 - \text{erc}(\lambda)$$

$$= 2/\pi \int_0^{\lambda} \exp(-\mu^2)\, d\mu$$

The agreement between the approximation, equation (19) and the exact solution, equation (21) seems to be quite good. For T(0,t), equation (21) is less than 1% higher.

Now the solution just described applies up to a time $t_v$. At $T(o,t_v) = T_v$ the vaporization time is

$$t_v = \{3(1 - 2e^{-1})/k\}\{KT_v/\alpha_o I_o\}^2 \qquad (22)$$

for $I_o/3KT_v \geq 1$.

CASE 2:

The laser pulse is a step function and the absorption coefficient increases linearly with the surface temperature up to the vaporization temperature $T_v$ according to the relation

$$\alpha = [\alpha + (\alpha_v - \alpha_o)][T(0,t)/T_v]$$

The solution of the heat flow equation (14) at $x = 0$ is then given by

$$T(0,t) = (\alpha - \alpha_o)T_v/\alpha_v - d_o \qquad (23)$$

with

$$\xi(t) = 3KT_o(\alpha - d_o)/[\alpha(\alpha_v - \alpha_o)I_o] \tag{24}$$

and $t_v$ is as before.

C. MATERIAL REMOVAL

Material removal begins with vaporization. As vaporization proceeds, the absorption of the laser beam increases rapidly as the depth of the crater increases. At first the evaporation rate and boundary temperature are equal to zero and all of the laser radiation is used in heating the opaque solid as pointed out in the previous section. If the external flux is intense enough, the surface will be brought to the vaporization temperature $T_v$ at time $t_v$. For later times, $t > t_v$, the problem is still defined by equation (6); but one of heat transfer in the presence of a moving phase boundary requiring new boundary conditions.

For the first boundary condition, the surface boundary energy balance relation, equation (7) must be changed to include a term to account for the energy expended on melting and vaporization. It must also account for the fact that the surface is no longer stationary.

$$-k \left.\frac{\partial T(x,t)}{\partial x}\right|_{x=x_s(t)} = \alpha I(t) - \rho L \frac{dx_s}{dt} \tag{25}$$

where $x_s(t)$ is the instantaneous position of the surface. For example, $x_s = 0$ when $t \leq t_v$. L is the effective latent heat of sublimation described by $L = L_{melt} + L_{vapor}$. The second boundary condition is as before, that is the target is assumed to be a semi-infinite solid

$$\lim_{x \to \infty} \frac{\partial T(x,t)}{\partial x} = 0 \tag{26}$$

The final condition is based on the temperature distribution in the material at $t_v$.

$$T(x,t) = f(x) \tag{27}$$

where the function f(x) is determined by the prevaporization solution.

With the boundary conditions just described, equation (6) becomes

$$\frac{d}{dt}\left( \int_{x_s}^{\ell} T \, dx \right) = \frac{k}{K}\left[\alpha I(t) - \rho L \frac{dx(t)}{dt}\right] - T_v \frac{dx_s(t)}{dt}$$

If $dx_s/dt = 0$ then equation (28) reduces to the prevaporization form, equation (13), as expected. The trial solution for the vaporization case may be chosen to be

$$T(x,t) = T_v\left[1 - \frac{x - x_s(t)}{\xi(t) - x_s(t)}\right]^2 \exp\left[-\frac{x - x_s(t)}{\xi(t) - x_s(t)}\right] \tag{29}$$

for $0 \leq x - x_s(t) \leq \xi(t) - x_s(t)$ and $T(x,t) = 0$ for $x - x_s(t) > \xi(t) - x_s(t)$. The surface temperature is fixed at $T_v$ as the position of the surface $x_s(t)$ moves into the solid. The surface recession velocity can be represented by

$$\dot{x}_s(t) = \frac{\alpha(T_v) I(T_v)}{\rho L}\left[\left(\frac{t}{t_v}\right) - 1\right]\left\{\left[1 - \frac{1}{2}\left(3 + \frac{CT_v}{L}\right)\right]\left[\left(\frac{t}{t_v}\right) - 1\right]\right\} \tag{30}$$

When the material is exposed to large constant flux and begins vaporizing after time $t_v$, the rate of material removed will approach a steady state as the corresponding surface recession velocity reaches a steady state.

$$\dot{x}_{ss} = \alpha(T_v) I(T_v)/\rho(L + CT_v) \tag{31}$$

The steady state penetration depth, $D(t)$, can now be written as

$$D_{ss} = k\rho L/KT_v = L/CT_v$$

Figure 7 from Ref. 30 depicts the normalized thermal penetration depth $D(t)$, surface position $x_s(t)$, and surface recession velocity $\dot{x}_s(t)$ for aluminum. Next the crater depth $\ell_c$ at a specific time $t_c$ can be determined from the integral equation

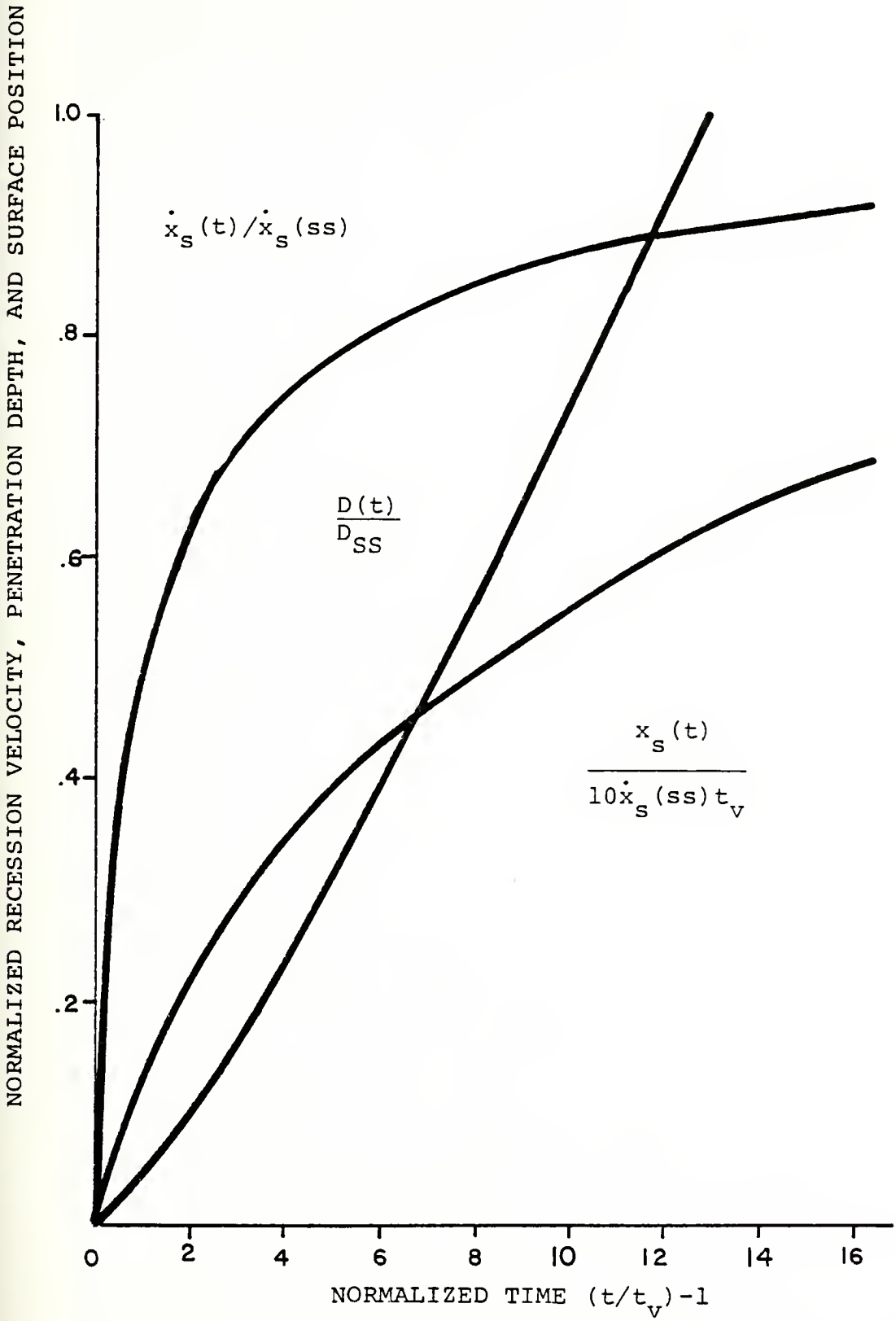


Figure 7. Time dependence of normalized values of surface recession velocity $\dot{x}_s(t)$, thermal penetration depth D(t), and surface position $x_s(t)$, for aluminum from Ref. 30.

$$\ell_c = \int_{t_v}^{t_c} \dot{x}_s(t)\, dt \qquad (32)$$

assuming that the target is effectively infinitely thick.

The previous discussion indicates how the temperature of a local spot on a target can be raised to the point where vaporization begins. At the same time, thermal diffusion begins as the local spot temperature rises. As a result, for most metals, the material is removed as a consequence of three processes: vaporization, the development of pressure in the cavity by vapor expansion and the creation of molten metal. Generally, vaporization begins at the surface. The initial velocity of a vapor jet flowing into a vacuum is equal to the local sound velocity. As the crater depth increases, the vapor velocity increases to a supersonic flow [4], which provides a mechanism for the washing of liquid metal from the walls of the crater. The fraction of material removed in the liquid state increases with pulse duration [21] because of the increase in temperature of the crater's inner walls with time.

Theoretical results are generally difficult to compare to experimental ones because of several factors. First, the amount of molten metal washed out of the crater and the initial fraction of absorbed energy is not well known. Next, a change in absorbed energy with temperature is generally unknown. And finally, estimates of the area on which the

beam was focused can involve considerable error. The distribution of illumination over a spot can be very nonuniform.

In addition, experimental results on the amount of material vaporized by a normal pulse laser exhibit considerable variation even for reported "similar conditions". The literature provides a number of sources where values of the amount of metal ejected by a normal pulse laser are given [59,58,11, 28,4,21,2].

Figure 8 depicts the ejected mass as a function of beam energy for a 700 μs duration pulse from a normal pulse neodymium glass laser [11]. The beam's total energy output was 1-15 joules and its spot size was $10^{-3}$ $cm^2$. In each case, material removal was accompanied by breakdown. The group of low melting metals experience larger amounts of material removed. Figure 8 shows that the amount of material ejected increases rapidly (exponentially) with increased energy. Chun and Rose conducted similar experiments a few years later [21]. Figure 9 shows the dependence of material removal on pulse duration at an average laser power of 30 KW. To obtain the data in Figure 9, they used different laser pulse durations but constant average laser power. The mass of the ejected material was determined by measuring the amount of material collected on the walls of a glass box surrounding the specimen.

In conclusion, one can say that the effect of normal pulse laser radiation on the surface of an opaque solid is a

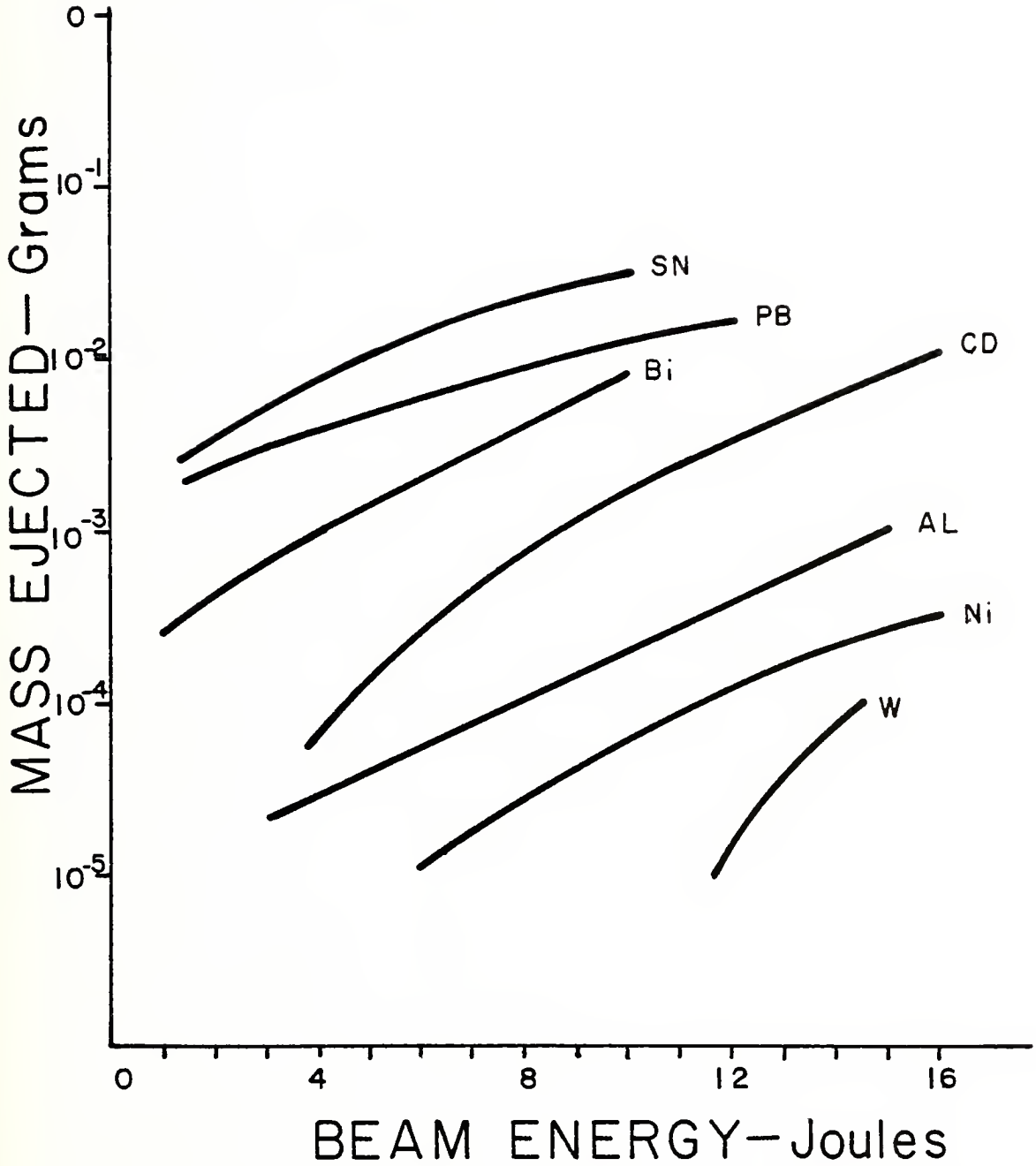


Figure 8. Experimental mass removal for various metals using a 700 μs Nd-glass laser focused to $10^{-3}$ $cm^2$ (Ref. 11).

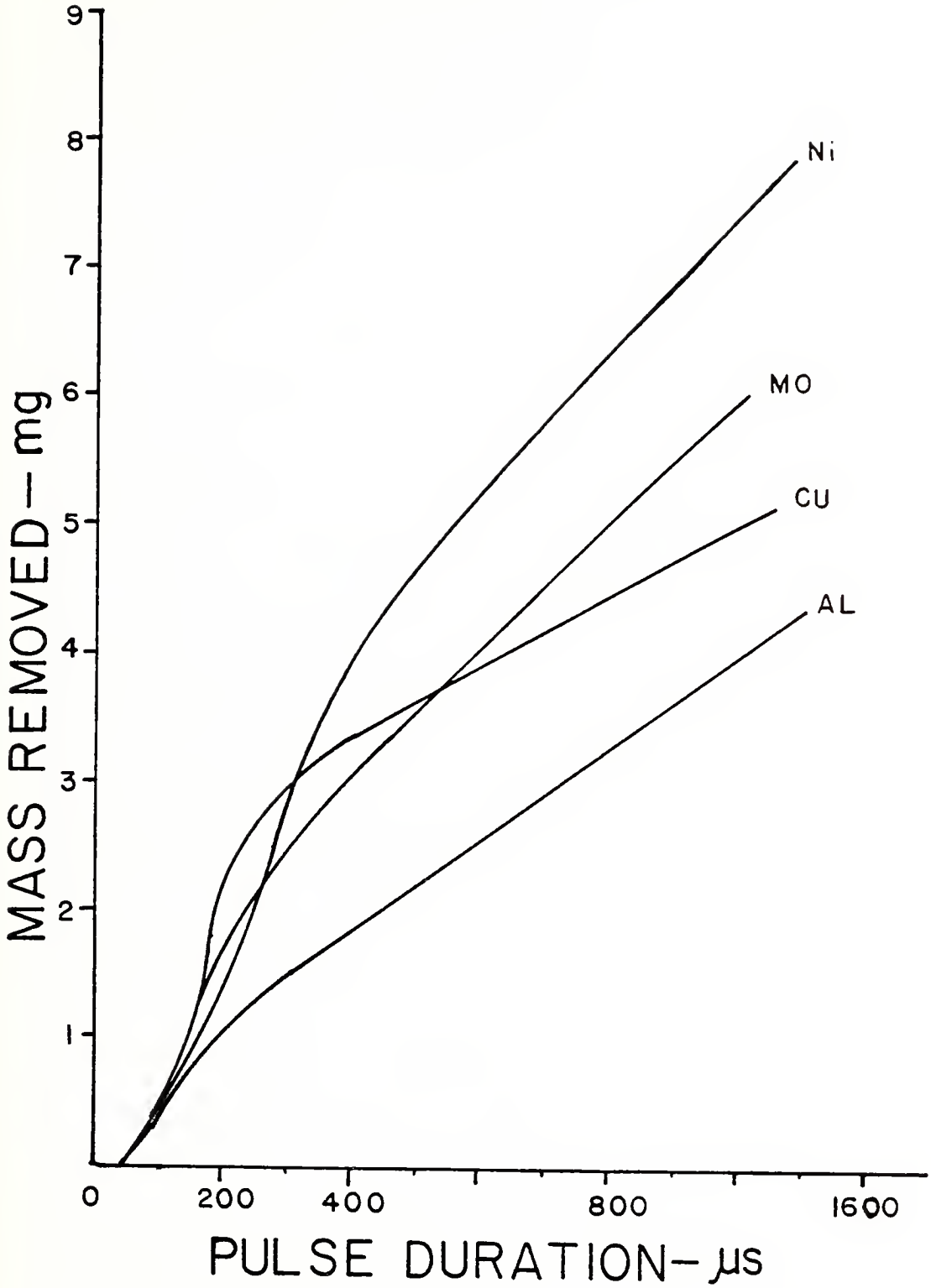


Figure 9. Time dependent material removal measurements. These measurements are the average weight of material removed from three specimens for laser pulses having an average power of $10^7 w/cm^2$ but different time durations (Ref. 21).

pronounced one. I have considered an ordinary thermodynamic approach for the calculation of the target temperature distribution, time to vaporization, and crater depth. Experimental results on material removal for lasers providing fluxes up to $10^6 - 10^7$ watts have been outlined. Representative values for mass removed and crater depth are on the order of a few milligrams and a few millimeters, respectively.

# III. EXPERIMENTAL DESIGN

## A. EQUIPMENT

The arrangement of the equipment utilized during this experiment is depicted in Figure 10.

### 1. Laser System

A neodymium glass laser emitting a wavelength of 1.06 micrometers was used for this experiment. The pockel's cell of the Korad K-1500 laser was replaced by a simple mirror to allow for normal pulse operation. Figure 11a shows a typical oscilloscope display of the laser pulse. Figure 11b is an expanded view of the same pulse to show the individual spikes. A detailed description of the laser system can be found in Appendix A of Ref. 55.

### 2. Target Chamber

The target chamber was made from a 6 inch cube of unbaked aluminum. Its internal volume is 12.9 ± .03 liters. The vacuum system using a mechanical forepump and an oil diffusion pump, was capable of providing chamber pressures on the order of $10^{-6}$ Torr. The target and ionization gauge were mounted as shown in Figure 12. The targets were made of 6062 aluminum, 50 mm in diameter and 7 mm thick. The surfaces were machined "smooth" on a metal lathe. A smaller target made from sheet aluminum (12mm x 20mm x .5mm) was also used. They were mounted on a holder described by Hwang [35].

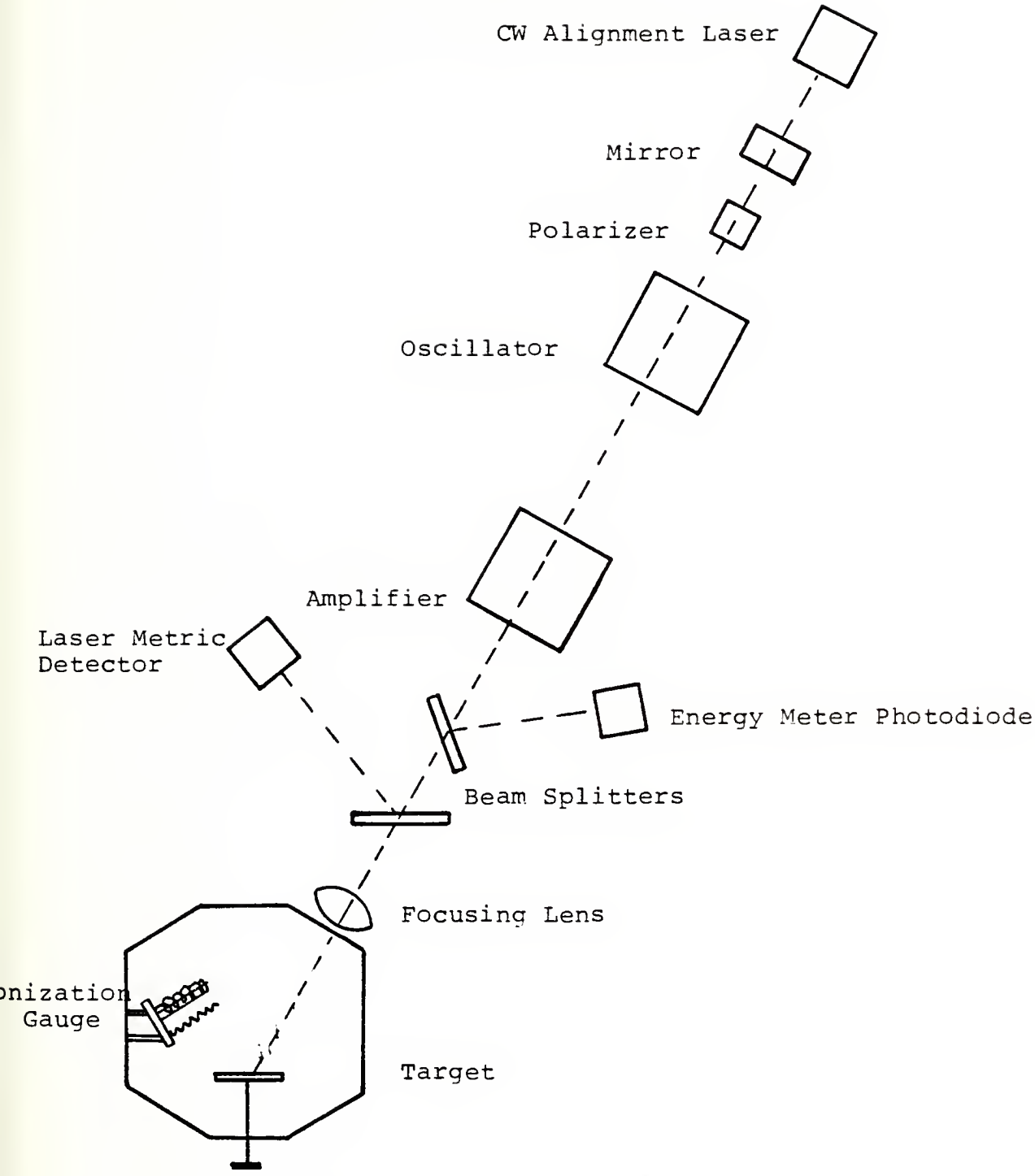


Figure 10. Block diagram of the general experimental equipment layout.

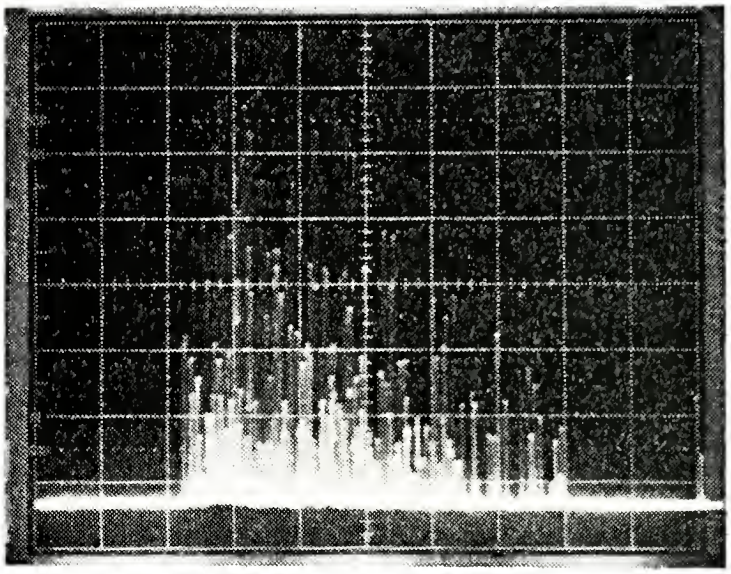

Figure 11a. Oscilloscope display of the laser pulse at 100 μs/div.

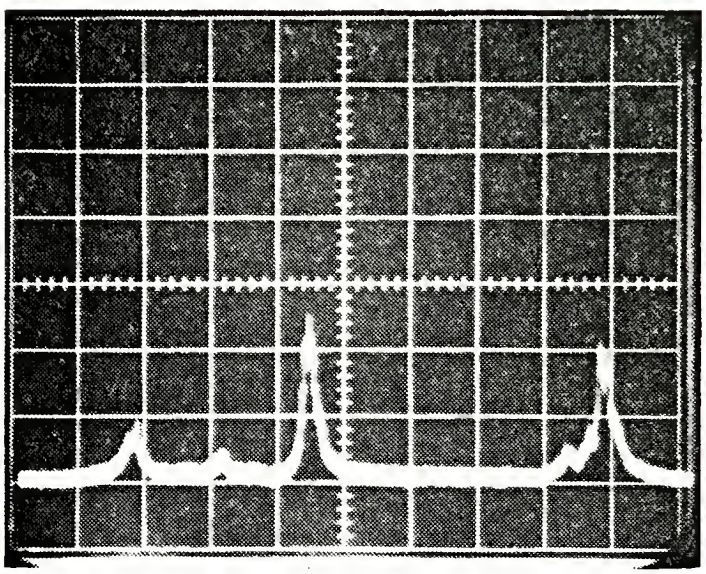

Figure 11b. Oscilloscope display of the laser pulse showing the individual spikes. Time is 2 μs/div.

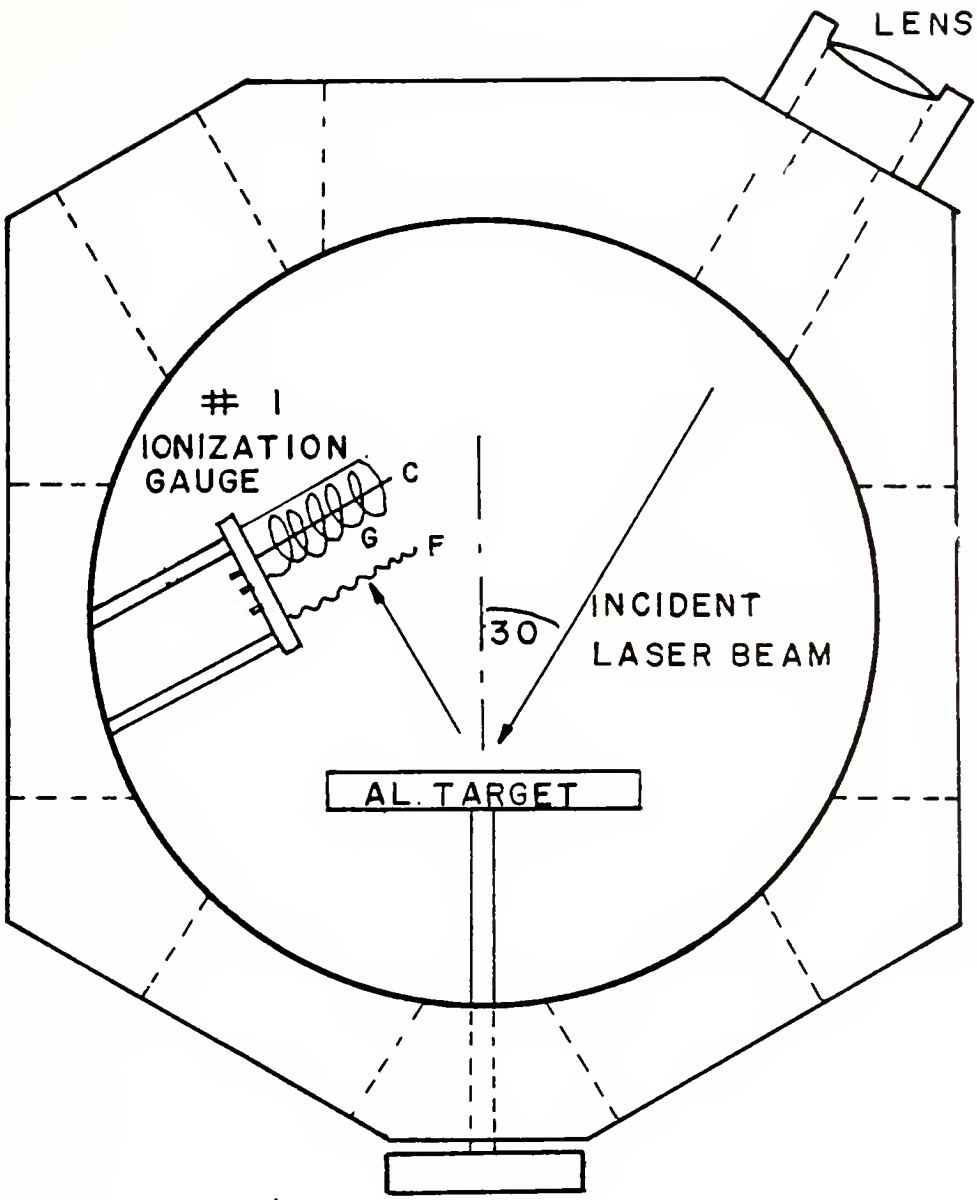


Figure 12. Top view of the target chamber. There is a port in the top of the chamber where the detector for the plasma radiation was located. C denotes the positive ion collector, G denotes the accelerating grid and F the Filament.

3. Ionization Gauge

A Hughes ionization gauge tube type 6578 was used as a device to measure the material ejected from the surface of the target. Gauge #1 was placed inside the target chamber in the path of the excited material. Gauge #2 was located below the target in the manifold to the chamber. Figure 13 pictures the gauge #1 plus mounting hardware. The gauge was designed with a very fine collector wire suspended in a cylindrical grid. A filament placed outside the grid is heated by passing a current (6 amps) through it. The grid cylinder, which has a positive potential applied to it, accelerates the electrons from the filament. A simple electric circuit for an ionization gauge is diagramed in Figure 14. There is a high probability that collisions between electrons and molecules will result in the formation of positive ions. Since the collector has a negative applied voltage, it collects ions within the grid area. The variations of collector current can then be measured and equated to the number of particles in the chamber [23]. If a plasma passes through the ion gauge, the collector will sense the positive ions resulting in an appropriate current increase. This is similar in operation to an electric probe used for plasma diagnostics [33].

4. Instrumentation

The laser output signal was sensed using a Lasermetric Series 3117, High Speed Detector. To protect the detector, 50, 5, and 1 percent transmission filters (at 1.06 μm) were placed in line with the radiation. The signal from the

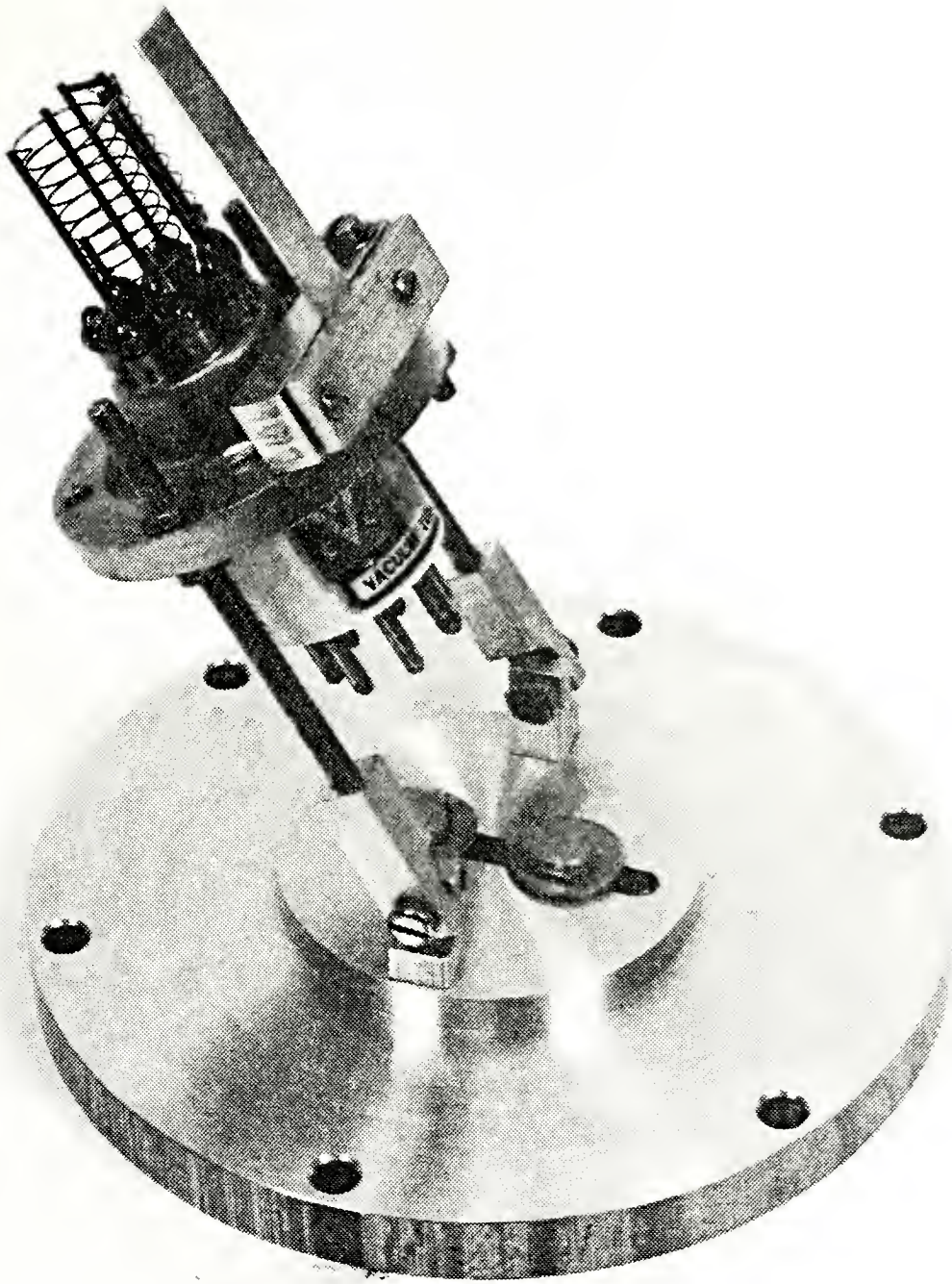

Figure 13. Hughes Ionization Gauge, gauge 1, with mounting hardware.

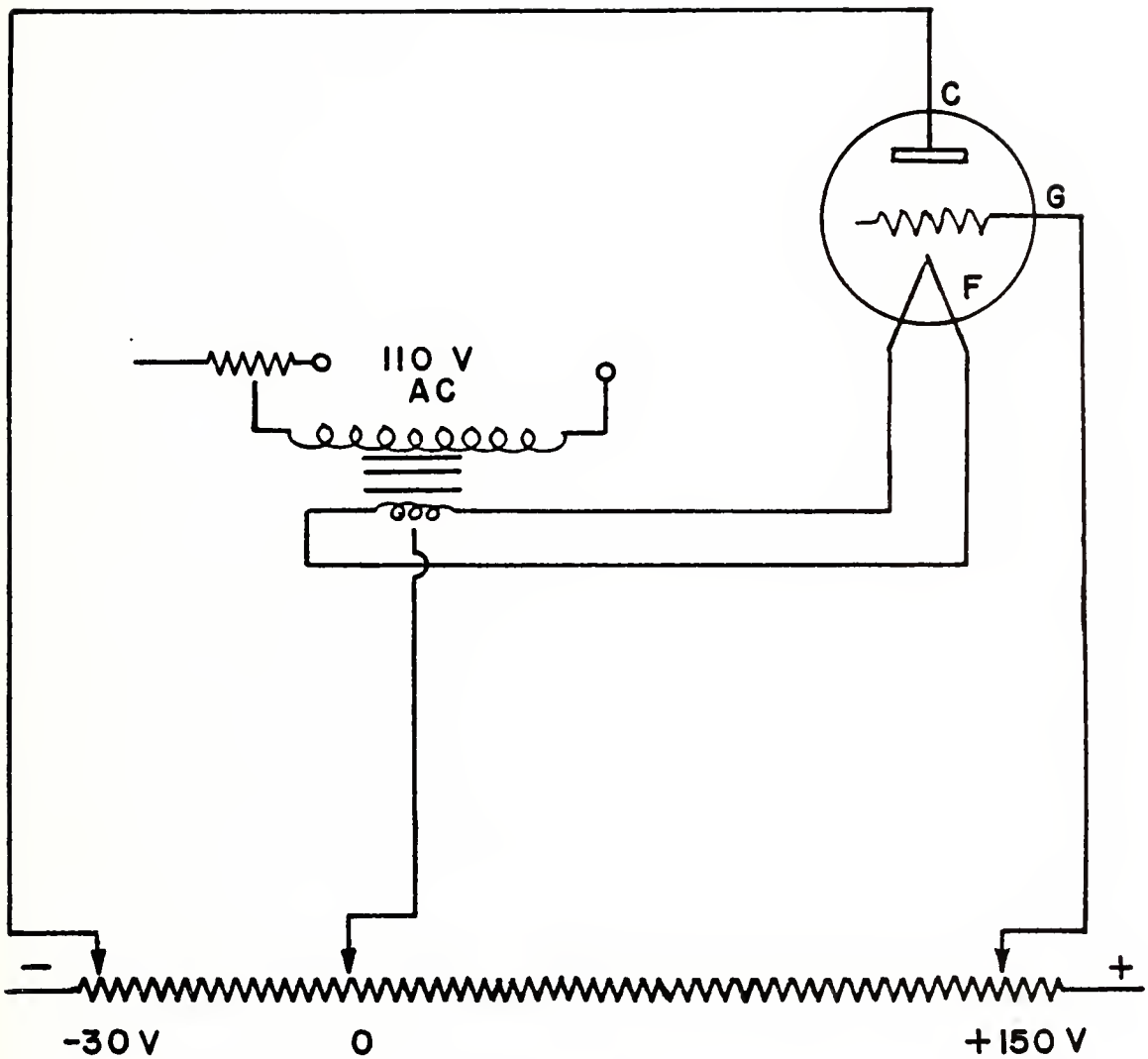


Figure 14. An example of a sample electrical circuit for an ionization gauge. C denotes the positive ion collector, G denotes the accelerating grid, and F the filament.

detector's high speed (< 150 picosecond) PIN diode was displayed on a Tektronix 7904 Oscilloscope. Total energy in the laser pulse was determined using a Laser Precision RK-3200 Series Pyroelectric Energy Meter. A 10 percent transmission filter (at 1.06 μm) was placed in front of the detector face, to insure that the level of intensity reaching the detector did not exceed the damage threshold of the detector. This instrument, which gave direct digital display of the total energy in a pulse, was calibrated using a Hadron Model 118 Thermopile. The calibration accuracy was no better than 20 percent which is to be expected [59].

The plasma radiation was detected using a Hewlitt Packard pin diode detector with response time < 1 nanosecond. To eliminate any signal from 1.06 μm radiation, a filter with optical density of 4.5 at 1.06 μm was placed over the face of the detector. The detector's signal was displayed on a Tektronix 7704 Oscilloscope.

The two ion gauges in the system, one in the chamber and one in the elbow beneath the chamber, were each connected to a Veeco Vacuum Gauge Control Panel. An oscilloscope was, in turn, connected to the recorder connection on each panel. The amplifier output was -2 volts with respect to the ground for a full scale pressure reading on all scales. A set of Granville-Phillips control panels was also used in lieu of the Veeco models. These control panels provided a -100 millivolt output for a full scale pressure reading on all scales.

Due to the singularity and duration of the pulses, all oscilloscope displays had to be recorded by photographing with the appropriate Tektronix camera. Polaroid 3000 speed black and white film was used exclusively.

Target weight measurements were made with a Cahn Electrobalance, Model DTL. This scale was capable of measurements as small as .01 milligrams with a reported accuracy to the nearest .01 milligram.

B. PROCEDURE

1. Ion Gauge Measurement Study

A target was affixed to the target holder and the chamber evacuated to about $10^{-6}$ Torr. Prior to taking data, all oscilloscopes and ionization gauges were adjusted and calibrated.

For all experiments the laser was set to provide an output of 15-18 Joules. The beam intensity (focus) was adjusted with a simple lens focusing system. A complete sequence of shots was taken varying the influence on the target, while measurements of the plasma and laser outputs and ionization gauge outputs were made. Some shots were repeated with gauge filament both off and on to distinguish the effect of the plasma on the collector current and to show the effect of the ionizing filament electrons.

2. Material Mass Study

The system was prepared and operated as before except that special small targets were used. The procedure began

by weighing a "standard" on the Electrobalance and recording the weight. The target sample was then weighed. After 5 or 6 laser shots on the target with the beam focused, it was reweighed. The "standard" was also reweighed to determine if the balance had "drifted". The difference in weight readings for the sample as well as the "standard" were recorded.

## IV. RESULTS AND DISCUSSION

One objective of this research was to find a method by which one could measure the amount of material ejected from a target irradiated by a laser beam. Initially, a Granville-Phillips ionization gauge control panel was used to monitor the ionization gauge signals, but was found to be unacceptable. The control panel's electronic circuits saturated when the laser was fired, yielding outputs that were not characteristic of the chamber pressure fluctuations. The data described was collected using Veeco control panels. Through the use of an ionization gauge installed in the target chamber, gauge 1, I was able to sense the plasma, neutral particles, and desorbed gases evaporated from the target surface. The reaction of the ionization gauge to each will be discussed below.

### A. PLASMA

When the 600 μs pulse was focused on an aluminum target, material was evaporated and a crater formed on the surface. The crater was oblong having dimensions of 2mm by 1mm by 0.5mm deep for pulses with energy 15-18 J. Assuming a conical shape for the crater, the calculated mass removed is 0.71 mg; however, not all of this material is vaporized. The crater was ringed with metal ejected from the crater. This metal was deposited on outer edges as a result of the

vapor flow scraping molten metal off of the inner cavity walls. A detailed display of the laser output and target plasma radiation from the same pulse is depicted in Figure 15. The beam was focused resulting in an energy density approximately 1.9 $x10^3$ $J/cm^2$. Light emission from the plasma was measured with a photo detector located on the top of the target chamber. A neodymium absorption filter was used to eliminate any direct radiation from the laser. Figure 15 indicates that, for this case, all of the laser spikes result in a plasma being generated. The laser spike is relatively symmetrical, but the plasma emission lineshape rises sharply as breakdown threshold is reached and then trails off exponentially as the plasma expands, cools, and recombines. There is also a good correlation between plasma radiation and the ionization gauge output. Figure 16 depicts these two traces for a single laser pulse which was defocused more than the pulse in Figure 15. Figure 16a shows breakdown spikes at $t_1$ = 0.38 ms and another at $t_2$ = 0.66 ms with approximately the same amplitude. The corresponding ionization gauge output can be seen in Figure 16b. The two plasma spikes at $t_1$ are manifested as one ionization gauge deflection. Both curves show an exponential decay. Of particular interest is the 0.8 μs amd 24 μs time for the 1/e decay of the plasma radiation and ionization gauge, respectively. When the gauge's filament was turned off, the signal displayed on the oscilloscope was the same. This is to be expected because the negatively biased collector acts like an ion collecting

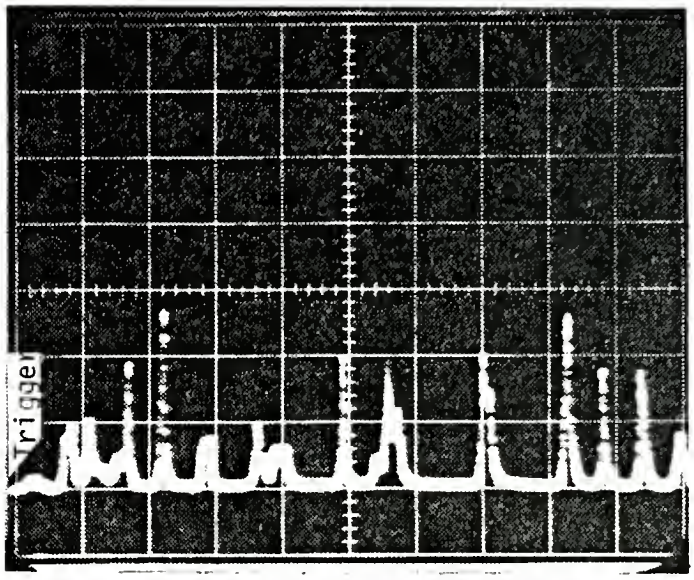


a. Oscilloscope trace of laser output at 1.06 μm.

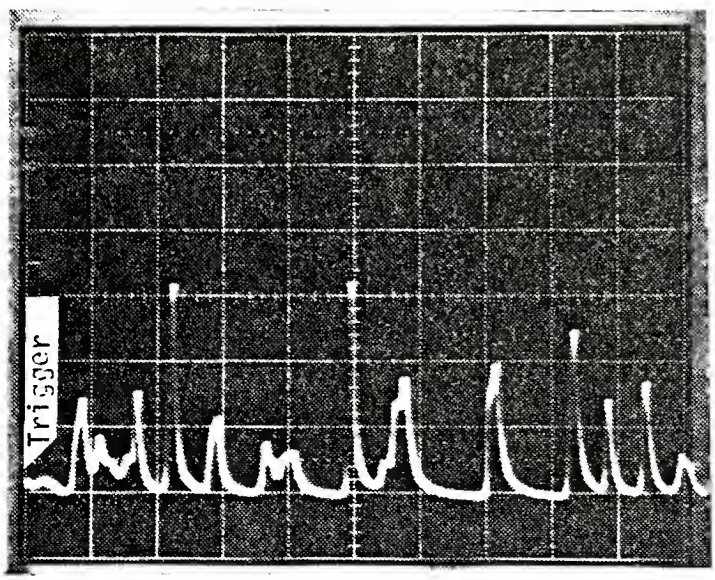


b. Oscilloscope trace of plasma radiation with 1.06 μm narrowband absorption filter in place.

Figure 15. Oscilloscope traces of laser output and plasma radiation taken from the same pulse. Trigger was delayed 0.22 ms. The pulse energy was 15 Joules. The beam was focused to approximately $8 \times 10^{-3}$ $cm^2$. Time reference for both traces was 5 μs/div.

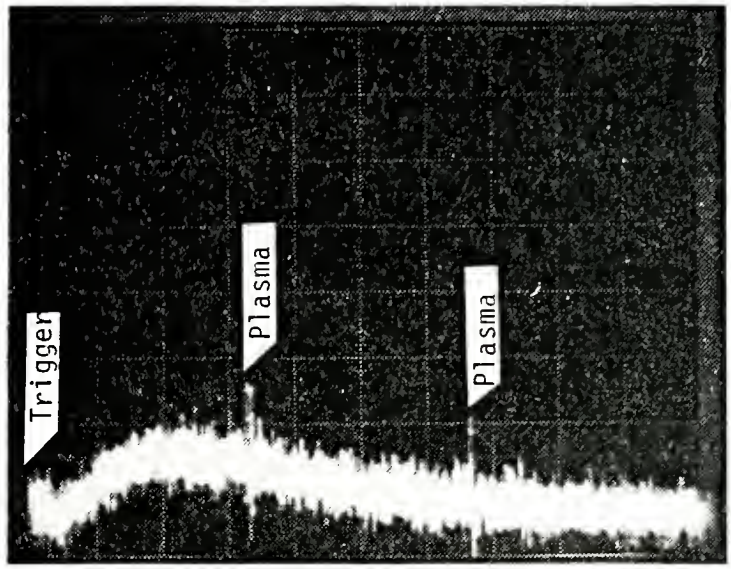


a. Oscilloscope trace of plasma light. The wide base signal is due to laser flash lamp radiation. The spikes above the background noise are light emitted from a breakdown plasma.

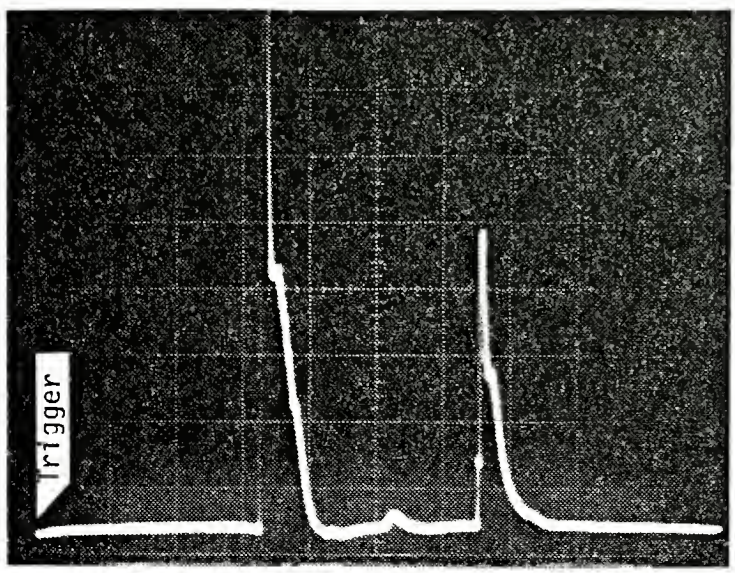


b. Oscilloscope trace of chamber ionization gauge output with filament on and control panel set on the $10^{-5}$ Torr range.

Figure 16. Oscilloscope traces of plasma radiation and ionization gauge output. The time for both traces was 0.1 ms/div.

electric probe. The plasma contains many ions which, in turn, provide a signal for the ionization gauge. Figure 16 also shows that there was no detectable time lag between plasma radiation and the corresponding ionization gauge signal. Actually, the plasma, traveling at about $2 \times 10^6$ cm/s [14], took approximately 5 μs to cross the 10.4 cm distance from the target to the collector, but this time was not perceivable on the 0.1 ms scale in Figure 16.

## B. DESORBED GASES

To demonstrate that the ionization gauge deflections measured "fly by" material, the laser beam was defocused to approximately $1.8 \times 10^{-2}$ $cm^2$. At this point, there was insufficient energy density, $J/cm^2$, to ionize, melt, or vaporize the target surface. Only gases were desorbed off of the surface. A visual inspection of the target showed a 0.4 cm diameter circle where the target had been heated. Figure 17 shows traces from the two different ionization gauges mounted in the system. The upper trace is from the chamber gauge, gauge 1, while the lower one corresponds to the gauge located below the chamber, gauge 2. The top trace shows a definite fluctuation, while the lower trace is relatively flat though its gain was 5 times greater. When the laser is fired several times in the same spot, the first three or four pulses caused a much higher positive pressure indication than subsequent ones. This effect has been previously reported [55,62]. It is due mainly to the desorption

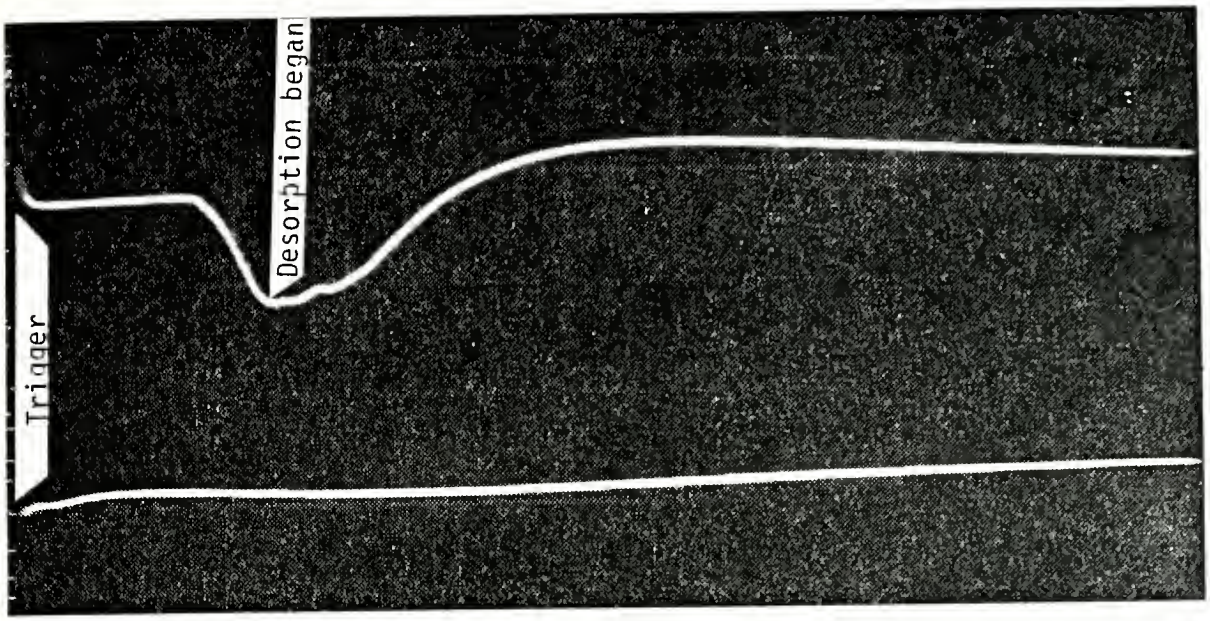


Figure 17. Oscilloscope display of the ionization gauge output with the control panel range set at $10^{-6}$ Torr range. The upper and lower displays are from gauge 1 and 2 respectively. The beam was defocued to 1.8 x $10^{-2}$ $cm^2$ (no plasma generation). Time was 0.2 ms/div. Gain was 1 V/div for the upper trace and 0.2 V/div. for the lower.

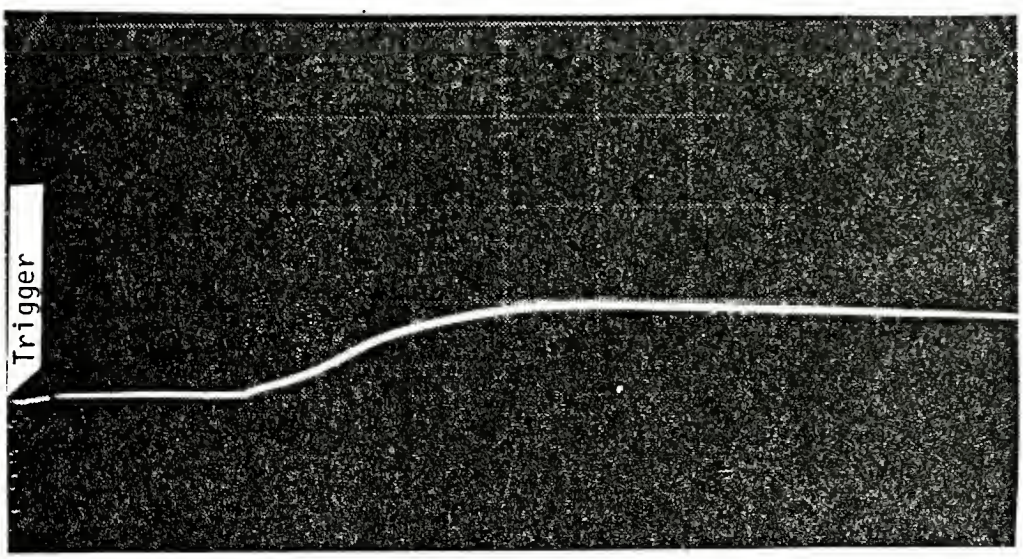


Figure 18. Oscilloscope trace of #1 ionization gauge. A 700 G horseshoe magnet was placed parallel to the target surface to deflect charged particles form the target surface. The beam with energy of 15 J was focused to approximately 1.8 x $10^{-2}$ $cm^2$. The reference for time was 0.2 ms/div. The control panel was set to operate on the $10^{-6}$ Torr range.

of impurities such as nitrogen, oxygen, hydrogen, water, and carbon dioxide found on the target surface.

A baffling result was the initial signal in the negative direction with the onset of lasing. If a magnet is placed adjacent to the target to deflect charges particles, the negative signal disappears and only a positive signal is seen, Figure 18. If the gauge's filament is turned off, the trace is flat for the same operaing conditions. No voltage drop on the +150 volt accelerating grid was observed. One explanation for the negative signal may be thermal or photo electron emission from the target surface. The gauge's filament has a negative space charge around it. The additional, probably more energetic, electrons from the target surface would increase the space charge and act as a shield returning (repel) thermal electrons back to the filament surface. The net effect is a reduction of the number of electrons accelerated by the grid. This, in turn, means less ionization takes place and therefore a drop in collector current. The positive portion of the trace, starting at the dips minimum, Figure 17, was due to the pressure increase by gases desorbed from the target surface. The conclusion that can be drawn is that the chamber ionization gauge was actually sensing what was flying past it.

## C. NEUTRAL PARTICLES

Neutral particles present a special problem of measurement. It was expected that electrons from the ionization

gauge's filament would ionize a fraction of the neutral aluminum particles allowing for their collection. This, in fact, happened. A comparison of Figure 19 and 20 shows that the neutral particles (and desorbed gases) were not collected if the filament was off, resulting in a steep decline and a flat trace after the plasma passed, Figure 20.

It was observed that when breakdown at the target surface occurred, plasma and neutral particles were ejected. The plasma velocity is on the order of $(kT_e/M_i)^{1/2}$, approximately $2 \times 10^6 - 2 \times 10^7$ cms, depending on the laser pulse parameters [14]. The plasma was therefore much faster than the neutral particles which leave the surface at the thermal velocity of $2 \times 10^4$ cms [59]. In Figure 19, this is demonstrated. The plasma passed the chamber ionization gauge first, immediately followed by the neutrals. The velocity of the neutral particles can be determined from the times depicted in Figure 21. The laser beam was focused to approximately 0.018 $cm^2$ and a 700 G horseshoe magnet placed next to the target to suppress thermal and photo electrons as previously discussed. A positive rise in the oscilloscope trace began at $t_2$ = 0.42 ms, 0.22 ms after lasing began, $t_1$. The first arriving neutral particles traveled the 10.4 cm from the target to the collector at $5.2 \times 10^4$ cm/s. The most probable thermal velocity of an aluminum particle leaving the target surface at the vaporization temperature of 2330 °K can be calculated from $(2Kt/M)^{1/2}$. It is $3.8 \times 10^4$ cm/s. The velocity of particles evaporated

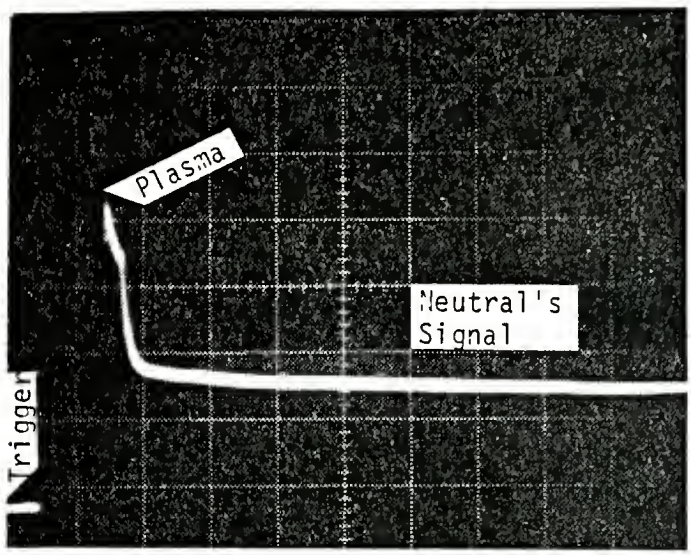


Figure 19. Oscilloscope display of the #1 ionization gauge output with filament on and with the control panel set on the $10^{-5}$ Torr range. Beam was focused down to 2 x $10^{-2}$ $cm^2$. Time is 0.5 ms/div.

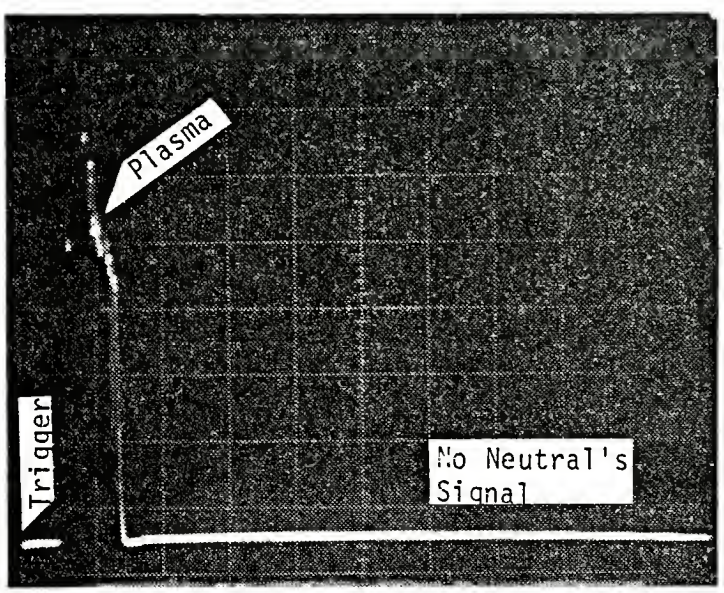


Figure 20. Ionization gauge oscilloscope trace for the same conditions as those in Figure 17 except that the filament current was turned off.

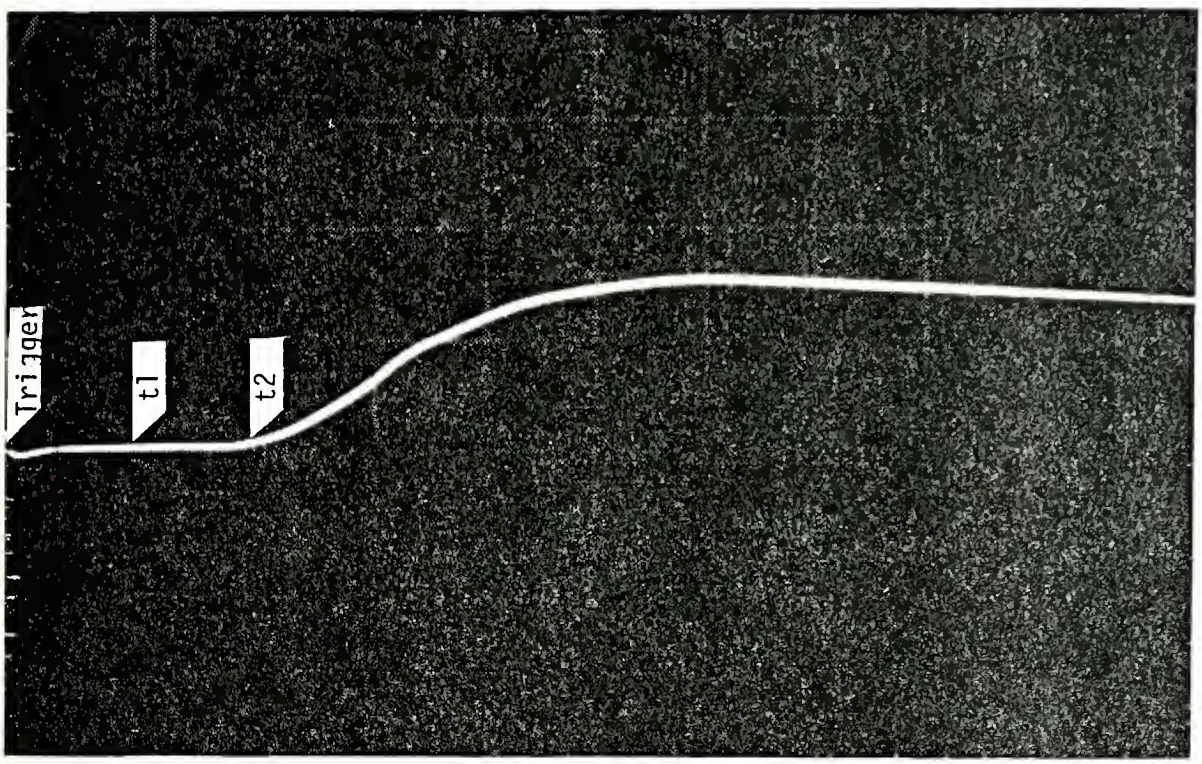


Figure 21. Oscilloscope trace of #1 ionization gauge. A 700 G horseshoe magnet was placed parallel to the target surface to deflect charged particles from the target surface. The beam with energy of 15 J was focused to approximately $1.8 \times 10^{-2}$ $cm^2$. The reference for time was 0.2 ms/div. The control panel was set to operate on the $10^{-5}$ Torr range.

from the surface can probably be characterized by a Maxwellian distribution. The faster experimental velocity value can be attributed to particles with velocities in the tail of the distribution.

Figure 22 depicts the results of a six shot sequence fired at one spot. Again, a magnet was used to deflect photon and thermal electrons away from the filament. The spot size of $1.8 \times 10^{-2}$ $cm^2$ and time scale of 0.22 ms/div were kept constant as the laser energy was increased from 18.8 to 36.6 Joules (18.8, 19.6, 20.5, 22.9, 24.6, and 36.6 Joules). The traces have increased amplitude with increased energy. The relative height of that portion of the curve attributed to neutral particle emission from the target was very dependent on laser flux. For all cases, positive deflections due to neutral particles occurred at the same time, $t_1$ = 0.42 ms. The final shot shows an initial spike, caused by a small plasma cloud, followed by a sharp rise due to neutral particles. One can conclude that as energy was increased, the initial arrival time of neutral particles at the collector remains constant. Further, the rise time decreased and the amplitude of the pressure signal increased as the beam energy density was increased.

As an example, Figure 23a depicts the ionization gauge signals as material, ejected from the target surface, passed by it. In this case, the experiment was conducted without the target magnet. Figure 23b is the corresponding trace of the plasma radiation. Both traces were from the same

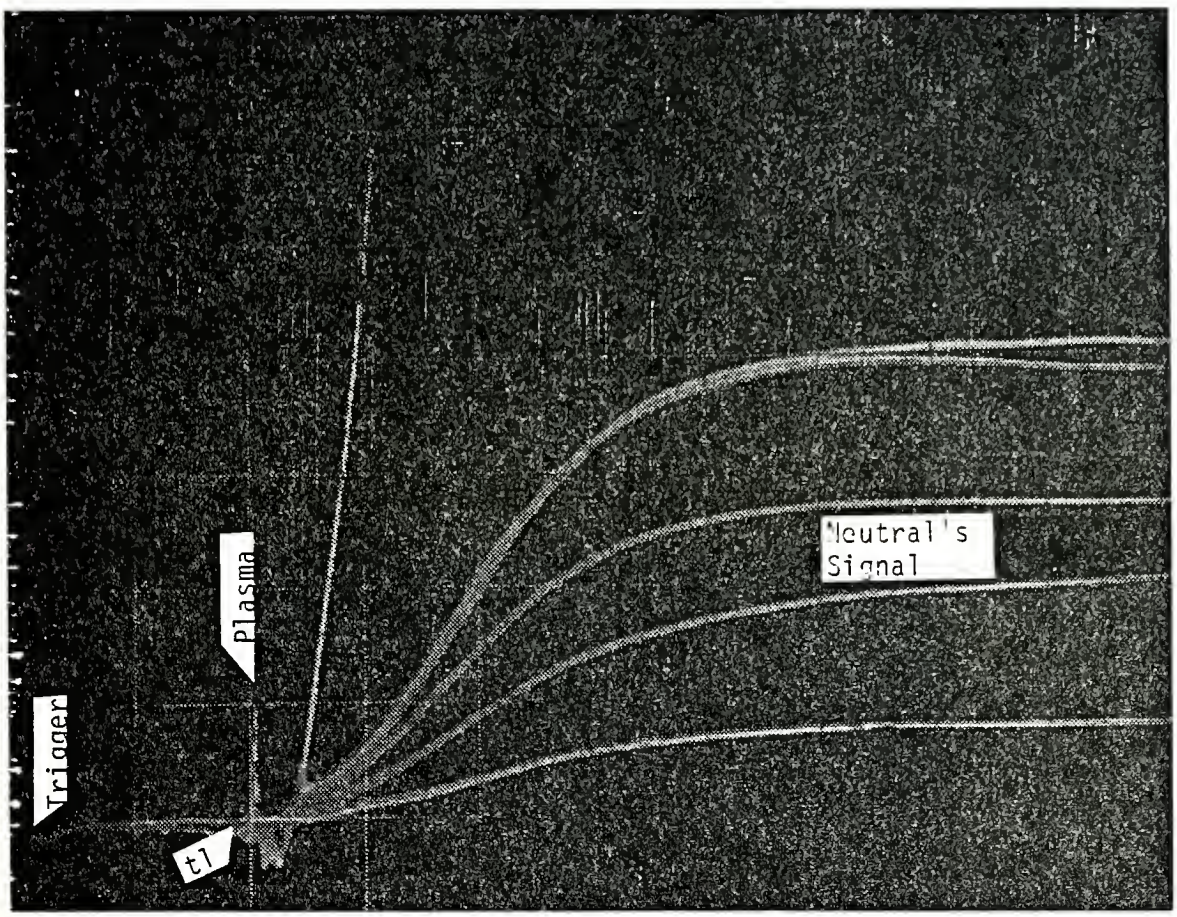


Figure 22. Oscilloscope trace of chamber ionization gauge. A 700 G magnet was placed parallel to the target. The laser beam was increased with each shot as the spot size, 1.8 x $10^{-2}$ $cm^2$, and the time, 0.2 ms/div. were kept constant. The gauge control panel was set on the $10^{-5}$ Torr range.

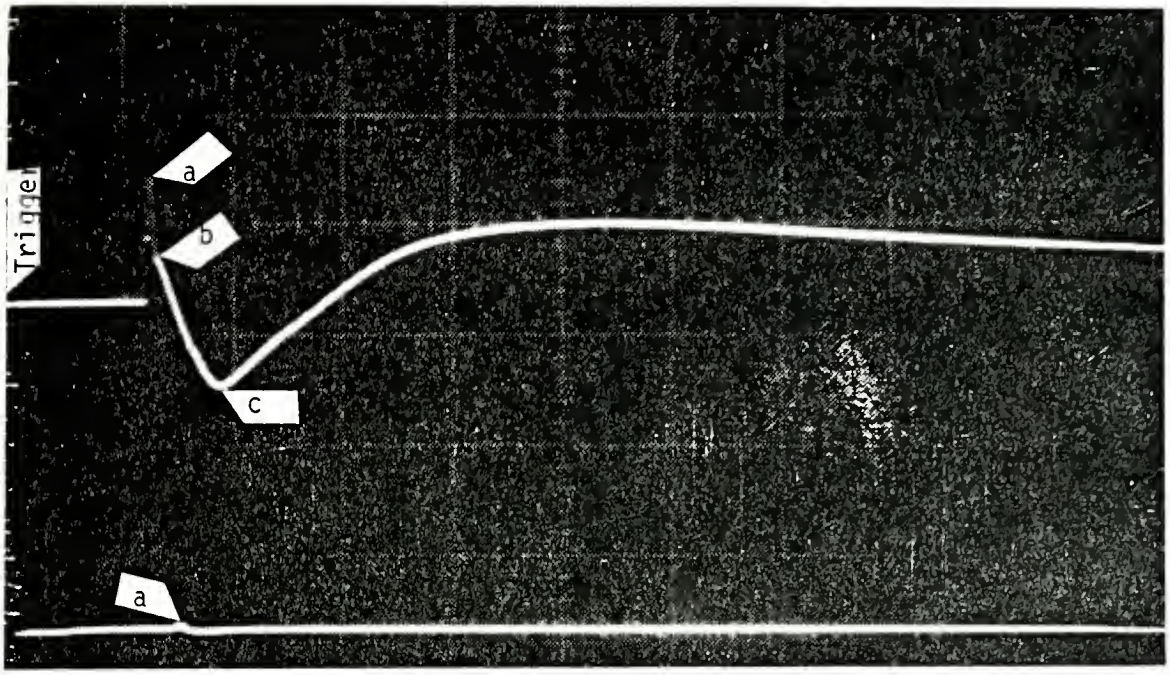


a. Oscilloscope display of ionization gauge output with control panel set on $10^{-5}$ Torr range. The lower trace is from gauge #2 with the filament off. The small ripple was due to plasma radiation. The upper trace is from the chamber gauge.

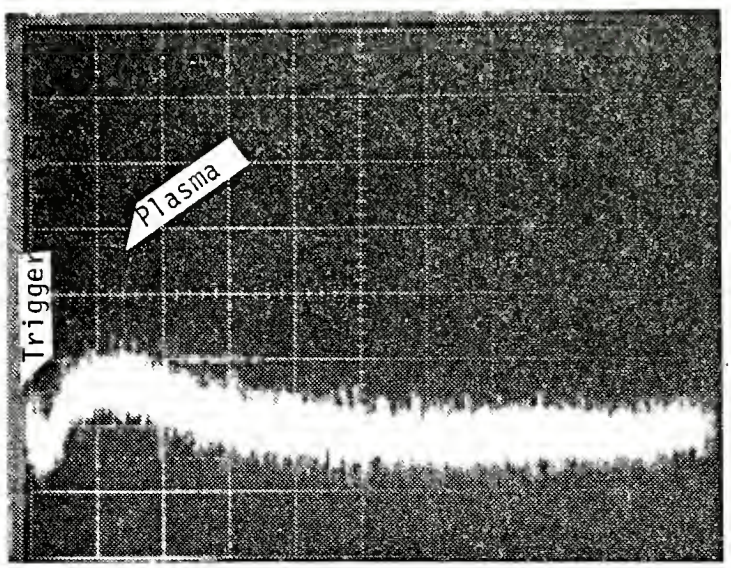


b. Oscilloscope trace of plasma radiation.

Figure 23. Oscilloscope displays of ionization gauge outputs and plasma radiation for the same shot. The beam which was defocused to approximately 2 x $10^{-2}$ $cm^2$ had energy of 18 J. The time reference for both displays was 0.2 ms/div.

laser pulse and had the same time scale of 0.2 ms/div. The pulse, with energy of 18 J, was focused to approximately $2 \times 10^{-2}$ $cm^2$. With the lasing starting at 0.22 ms, Figure 23b shows a plasma spike at 0.24 ms. The upper and lower ionization gauge traces also show the plasma signal, point a. When the plasma expands and cools, i.e., after cessation of the plasma spike, the predominant signal in the negative direction was from the photo or thermal electrons emitted from the laser heated surface, segment b-c. Neutral particles which have a slower velocity than the electrons, arrived at the gauge last causing an up-swing in the trace to the right of point c. For a case of more intense laser radiation, consider Figure 24. The beam had about the same energy, 19.5 J, but it had been focused to provide breakdown as depicted in Figure 24b. Both traces had a time scale of 0.2 ms/div. to facilitate comparison. The gauge trace shows a "wild" deflection as the plasma passed through, segment a-b. At point b, breakdown processes ceased but lasing continued, still adding energy to the hot surface. The segment b-c shows a gradual decline in the number of neutral particles ejected from the surface. Conversely, when lasings stops, vaporization stops and there was a rapid fall in the curve, segment c-d. This was due to the rapid surface cooling of the target.

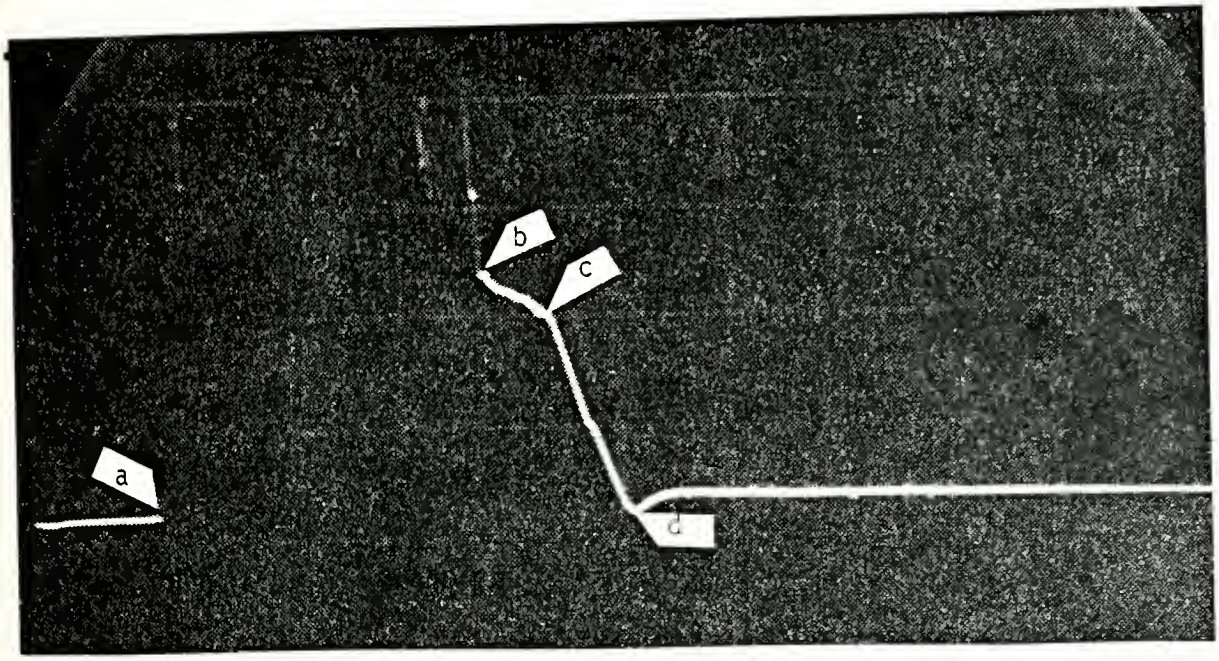


a. Oscilloscope display of #1 ionization gauge output. Control panel range was set on $10^{-5}$ Torr range.

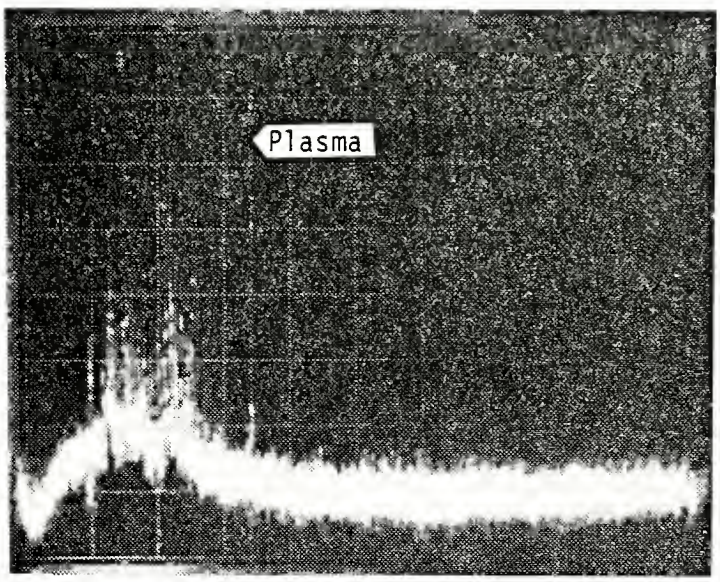


b. Oscilloscope trace of plasma radiation.

Figure 24. Oscilloscope displays of ionization gauge output and plasma radiation for the same shot. The beam was focused from that in Figure 22. Energy was approximately 18 J. Time reference was 0.2 ms/div. for both displays.

## D. MASS OF MATERIAL REMOVED

In order to equate the chamber ionization gauge signal to a specific number of particles ejected or ultimately the mass of the material removed, one must first be able to measure the mass of the ejected material. Small aluminum targets were weighed and places in the target chamber. The laser, with energy about 18 J, was fired at five locations on each target. Beam spot size was approximately 0.016 $cm^2$. The target craters were approximately 0.5 mm deep and had the usual metal splashed around the periphery of the crater. From the volume of the crater, the estimated mass removed was 0.7 mg. However, upon trying to reweigh the target, it was found that only a few hundredths of a milligram of material seem to have been removed. Compared to previous experimental work, this amount seems to be extremely low [11,21]. One explanation may be the difficulty encountered in weighting small amounts. The Electrobalance used to weigh the targets tended to drift. Fluctuations varied from hundredths to tenths of milligrams for the same sample. A standard weight was used to eliminate some of the drift, but only the long term effects could be eliminated. As a consequence, the mass of material removed was not accurately determined.

## V. CONCLUSIONS

Laser induced evaporation of material from a target surface has been investigated using a normal pulse laser. The technique of using an ionization gauge to sense the ejected materials does work. The gauge essentially "sees" what is flying past it. When breakdown on the target surface occurs, a crater is formed. The breakdown is accompanied by generation of a plasma and neutral particles. Breakdown can be avoided by defocusing the laser to a larger spot on the target surface. In this case, only gas desorption from the surface occurs and much smaller signals are observed with the ionization gauge.

A good correlation between incident radiation, plasma radiation, and the ionization gauge fluctuations was observed. For laser energy densities sufficient to cause many breakdowns on the target surface, the ionization gauge reacts with large positive signals to the plasma which arrives first, and then to the slower velocity neutral particles. From time-of-flight measurements the first arriving neutral particle velocity was determined to be $5.2 \times 10^4$ cm/s which compares favorably with published data. For less intense laser radiation, surface breakdown did not occur or occurred only weakly a few times during a normal laser pulse. For this case, the ionization gauge initially gave a negative signal in conjunction with the onset of lasing (excluding positive

plasma caused fluctuations). This can be attributed to thermal and photo electrons ejected from the target surface. Once the slower velocity neutral particles (and desorbed gases) arrive at the gauge, the signal increases and becomes positive. The signal amplitude is commensurate with the laser energy density.

Mass removal measurements were inconclusive. Experimental measurements of crater volume indicated that .017 mg of aluminum were removed; however, some of this material was deposited in a ring around the crater opening. Further experimental work needs to be done on weighing the mass ejected from the target surface. Once an acceptable technique is developed, then correlation experiments between the weight of the mass removed and ionization gauge fluctuations should be conducted to "calibrate" the ionization gauge output.

## BIBLIOGRAPHY


1. Aerospace Corporation Report TR-1001 (2210-10)-2, Chemistry of Wire Explosions in Hydrocarbons, by B. Siegel and R.L. Johnson, September 1966.

2. Akimov, A. J. and Mirken, L. I., "Certain Regularities in the Effects of Laser Beams on Pure Metals," Soviet Physics-Doklady, v. 13, p. 1162-1164, May 1969.

3. Air Force Cambridge Research Laboratories Report 68, A Bibliography of the Electrically Exploded Conductor Phenomenon. W. G. Chace, and E. M. Watson, October 1967.

4. Anisimov, S. J., and others, "Effects of Powerful Light Fluxes on Metals," Soviet Physics-Technical Physics, v. 11, p. 945-952, January 1967.

5. Anisimov, S. I., "Evaporation of a Light-Absorbing Metal," High Temperature, v. 6, p. 110-114, 1968.

6. Basov, N. G., and others, "Reduction of Reflection Coefficients for Intense Laser Radiation on Solid Surfaces," Soviet Physics-Technical Physics, v. 13, p. 1581-1582, May 1969.

7. Bechtel, J. H., "Heating of Solid Targets With Laser Pulses," Journal of Applied Physics, v. 46, p. 1585-1593.

8. Bhattacharta, M. G., Craig, J. P., and Frost, T. F., Radiation Generation From Exploding Wires, Dept of Electrical Engineering, Texas Tech University, August 1976.

9. Boeing Company Document #D2-90094, Exploding Foils - The Production of Shock Waves and The Acceleration of Thin Plates, by D. V. Keller and J. R. Penning, Jr., December 1966.

10. Bonch-Bruevich, A. M., and others, "Effects of a Laser Pulse on The Reflecting Power of a Metal," Soviet Physics-Technical Physics, v. 13, p. 640-643, November 1968.

11. Braginskii, V. B., Minakova, J. I., and Rudenko, V. N., "Mechanical Effects in the Interaction Between Pulsed Electrical Radiation and a Metal," Soviet Physics-Technical Physics, v. 12, p. 753-757, December 1967.

12. Burkhalter, P. G. and Dozier, C. M., "X-ray Line Emission and Plasma Conditions in Exploding FE Wires," Journal of Applied Physics, v. 49, p. 1092-1098, March 1978.

13. Burkhalter, P. G., Dozier, C. M., and Nagel, D. J., "X-ray Spectra from Exposed-Wire Plasmas," Physical Review, v. 15, p. 700-717, February 1977.

14. Callahan, P. J., Laser Plasma Particle Velocities, M.S. Thesis, U. S. Naval Postgraduate School, 1976.

15. Carslaw, H. S. and Jaeger, J. C., Conduction of Heat in Solids, 2nd ed., pp. 10, 263-265, Oxford University Press, 1959.

16. Caruso, A., "Interaction of Intense Light Pulses with Solid Materials," (In: Physics of High Energy Density), p. 353-354, Academic Press, 1971.

17. Chase, W. G. and Moore, H. K., Exploding Wires, v. 1, p. 7-8, Plenum Press, Inc., 1959.

18. Chase, W. G. and Moore, H. K., Exploding Wires, v. 2, Plenum Press Inc., 1962.

19. Chase, W. G. and Moore, H. K., Exploding Wires, v. 3, Plenum Press Inc., 1964.

20. Chase, W. G., and Moore, H. K. Exploding Wires, v. 4, Plenum Press Inc., 1968.

21. Chun, M. K. and Rose, K., "Interaction of High-Intensity Laser Beams with Metal," Journal of Applied Physics, v. 41, p. 614-620, February 1970.

22. Dozier, C. M., and others, "High Ionization States in Exploding-Wire Plasma," Journal Physics, Atomic Molecular Physics, v. 10, p. 673-677, 1977.

23. Dushman, S., Scientific Foundations of Vacuum Techniques, 2nd ed., p. 301-353, Wiley, 1962.

24. Duston, P. and Duberstadt, J., "X-ray Emission From Laser-Heated Exploding Wires," Physical Review, v. 18, p. 1707-1716, October 1978.

25. Goodman, T. R., "The Heat Balance Integral And Its Application to Problems Involving a Change of Phase," (In: Heat Transfer And Fluid Mechanics Institute Conference), June 1957.

26. Goodman, T. R., "Application On Integral Methods To Transient Non Linear Heat Transfer," (In: Advance in Heat Transfer), p. 51-122, Academic Press, 1964.

27. Grabatin, H. and Steffens, H., "A New Method For Surface Coating-Use The Exploding Wire Phenomenon," Surface Technology Yearbook, v. 32, p. 257-265, 1976.

28. Grechikhin, L. I. and Min'Ko, L. Ya., "Similarity Between Physical Processes in A Pulsed Discharge and in the Effect of Laser Radiation on a Metal," Soviet Physics-Technical Physics, v. 12, p. 846-849, December 1967.

29. Griem, H. R., Plasma Spectroscopy, p. 193-202, McGraw-Hill, 1964.

30. Harrach, R. J., "Analytical Solutions For Laser Heating and Burn Through of Opaque Solid Slabs," Journal of Applied Physics, v. 48, p. 2370-2383, June 1977.

31. Harrach, R. J., "Estimates on the Ignition of High-Explosives by Laser Pulses," Journal of Applied Physics, v. 47, p. 2473-2482, June 1976.

32. Holman, J. Pl, Heat Transfer, 4th ed., p. 2-4, McGraw-Hill, 1976.

33. Huddlestone, R. H., and Leonard, S. L., Plasma Diagnostic Techniques, p. 113-117, Academic Press, 1965.

34. Hughes, T. P. Plasmas and Laser Light, p. 26-28, Wiley, 1975.

35. Hwang, Z. W., Laser Induced Evaporation From Stainless Steel Surfaces, M. S. Thesis, U. S. Naval Postgraduate School, 1978.

36. Kagavov, M. I., Lifshitz, I. M., and Tanatarov, L. V., "Relaxation Between Electrons and the Crystalline Lattice," Soviet Physics - JETP, v. 4, p. 173-178, March 1957.

37. Koy, P., Mathematical Description of Exploding Wires, Akademie Die Wissenschaften Berlin Monatsberichte, v. 9, p. 1-16, 1967.

38. Krokhin, O. N., "High Temperature and Plasma Phenomena Induced by Laser Radiation," (In: Physics Of High Energy Density), p. 278-305, Academic Press, 1971.

39. Landau, H. G., "Heat Conduction In A Solid," Quarterly Journal Of Applied Mathematics, v. 8, p. 81-94, January 1950.

40. Lawrence Livermore Laboratory Report UCRL - 52389, Theory For Laser-Induced Breakdown Over A Vaporizing Target Surface, by R. J. Harrach, December 1977.

41. Levine, L. S. and Vitkovitsky, I. M., "Pulsed Power Technology for Controlled Thermo-Nuclear Fusion," IEEE Transactions On Nuclear Science, v. WS-18, p. 255-264, August 1971.

42. Lockheed Missiles and Space Company, Inc., Report D352890, A Theoretical Study of Laser-Target Interaction, by P. D. Thomas and H. M. Musal, 31 August 1973.

43. McKelvey, J. P., Solid State and Semiconductor Physics, p. 180-207, Harper and Row, 1966.

44. Mott, N. F., The Theory of the Properties of Metals and Alloys, p. 99-103, Oxford Univeristy, 1936.

45. Nairne, E., "Electrical Experiments," Phil Trans Roy Society, London v. 64, p. 79-89, 1976.

46. Naval Ordnance Laboratory Report NOLTR-66-144, Ignition Of Explosives By Exploding Wires, by H. S. Leopold, September 1966.

47. Naval Research Laboratory Report 3840, Dynamics and Radiative Yields from Aluminum Multiple Wire Arrays, by D. G. Colombant, M. Lampe, and J. Davis, August 1978.

48. Naval Research Laboratory Report 10, "Exploding Wire Research 1774-1963," by J. R. McGrath, May 1966.

49. Naval Research Laboratory Report 7728, Response of Materials To Laser Radiation: A Short Course, by J. T. Schriempt, 10 July 1974.

50. Naval Research Laboratory Report MR3760, Use of Multiple Photo-Excitation In An Optically Thick Silicon-Aluminum Plasma To Obtain Lasing at 44A, by J. P. Apruzese, K. G. Whitney, and Davis, April 1978.

51. Naval Research Laboratory Report 3726, WHYRAC, A New Modular One-Dimensional Exploding Wire Code, by D. G. Colombant and M. Lampe, February 1978.

52. Naval Research Laboratory Report #2666, X Radiation From High Energy Density Exploded Wire Discharges, by P. Mosher and others, October, 1973.

53. Physics International Report PIFE-069, Exploding Fine Wires, by W. T. Link, S. Putnam and J. Creighton, June 18, 1968.

54. Physical Science, Inc. Report PSI TR-15, Analytical Solutions for Initiation of Plasma Absorption Above Laser Irradiated Surfaces, by A. N. Pirri, October 1974.

55. Polk, J. S., Laser Induced Desorption Of Gas From Stainless Steel, M. S. Thesis, Naval Postgraduate School, 1977.

56. Prokhorov, A. M., Batanov, V. A. Bunkin, F. V., and Fedorov, V. B., "Metal Evaporation Under Powerful Optical Radiation," IEEE Journal of Quantum Electronics, v. QE-9, May 1973.

57. Ready, J. F., "Charge of Reflectivity of Metallic Surfaces During Irradiation by $CO_2$-Tea Laser Pulses," IEEE Journal of Quantum Electronics, v. QE-12, p. 137-142, February 1976.

58. Ready, J. F., "Effects Due to Absorption of Laser Radiation," Journal of Applied Physics, v. 36, p. 462-468, February 1965.

59. Ready, J. F., Effects of High Power Laser Radiation, Academic Press, 1971.

60. Redstone Scientific Information Center Report RSIC-481, Exploding Foil Techniques: A Bibliography, by W. H. Hoop, 28 October 1965.

61. Rubanova, G. M., and Sokolov, A. P., "Metal Heating by Laser Radiation," Soviet Physics-Technical Physics, v. 12, p. 1226-1228, March 1968.

62. Schwirzke, F., Brinkschulte, H., and Hashmi, M., "Laser Induced Desorption of Gas from Metallic Surfaces," Journal of Applied Physics, v. 46, p. 4891-4894, November 1975.

63. Shipman, J. D., "The Electrical Design of the NRL Gamble II, 100 KiloJoule, 50 Nanosecond, Water Dielectric Pulse Generator Used in Electron Beam Experiments," IEEE Transactions on Nuclear Science, v. NS-18, p. 243-246, Aug 1971.

64. Smith, D. C., "Gas Breakdown Initiated by Laser Radiation Interaction with Aerosols and Solid Surfaces," Journal of Applied Physics, v. 48, p. 2217-2225, 6 June 1977.

65. Sparks, M., "Theory of Laser Heating of Solids: Metals," Journal of Applied Physics, v. 47, p. 837-849, March 1976.

66. Ujihara, K., "Reflectivity of Metals at High Temperatures," Journal of Applied Physics, v. 43, p. 2376-2383, May 1972.

67. U. S. Army Missile Command Report RS-TK-70-3, Exploding Foil Techniques, by E. H. Richert and W. S. Hodge, 23 April 1970.

68. Veiko, V. P., and others, "Metal Temperature in Interaction Region with a Laser Beam," Soviet Physics-Technical Physics, v. 12, p. 1410-1412, April 1963.

69. Vlastos, A. E., "Electrical Explosiosn of Tungsten Wires in a Vacuum," Journal of Applied Physics, v. 44, p. 108-112, January 1973.

70. Wei, P. S., Nelson, D. J., and Hall, R. B., "Laser-Induced Evaporation of Solid Surfaces," Journal of Chemical Physics, v. 62, p. 3050-3051, April 1975.

71. Zavecz, T. E., and Saifi, M. A., "Metal Reflectivity Under High-Intensity Optical Radiation," Applied Physics Letters, v. 26, p. 165-168, 15 February 1975.

72. Ziman, J. M., Electrons and Phonons, p. 175-219, Oxford University Press, 1960.

73. Ziman, J. M., Electrons and Phonons, p. 321-322, Oxford University Press, 1960.

74. Ziman, J. M., Principles of the Theory of Solids, p. 219-250, Cambridge Press, 1964.

## INITIAL DISTRIBUTION LIST

| | | No. Copies |
|---|---|---|
| 1. | Defense Documentation Center<br>Cameron Station<br>Alexandria, Virginia 22314 | 2 |
| 2. | Library, Code 0142<br>Naval Postgraduate School<br>Monterey, California 93940 | 2 |
| 3. | Department Chairman, Code 61Wh<br>Department of Physics and Chemistry<br>Naval Postgraduate School<br>Monterey, California 93940 | 1 |
| 4. | Assoc. Prof. F. R. Schwirzke, Code 61Sw<br>Department of Physics and Chemistry<br>Naval Postgraduate School<br>Monterey, California 93940 | 3 |
| 5. | Major Chris B. Johnson<br>5273 Felicia Avenue<br>Livermore, California 94550 | 1 |
| 6. | Director Defense Nuclear Agency<br>Washington, D. C. 20305<br>Attn: W. E. Murray, LTC, USA, F&AO | 1 |

Thesis
J5745 Johnson
c.1
186733
Induced evaporation of metal from an aluminum surface by a normal pulse neodymium laser.